Journal of Materials Chemistry A

Accepted Manuscript

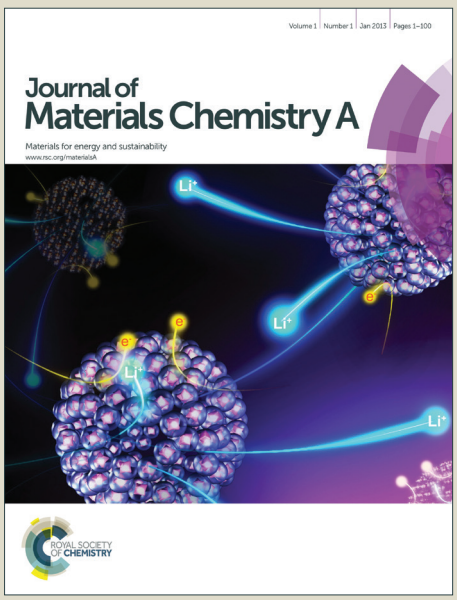

ROYAL SOCIETY OF CHEMISTRY

www.rsc.org/materialsA

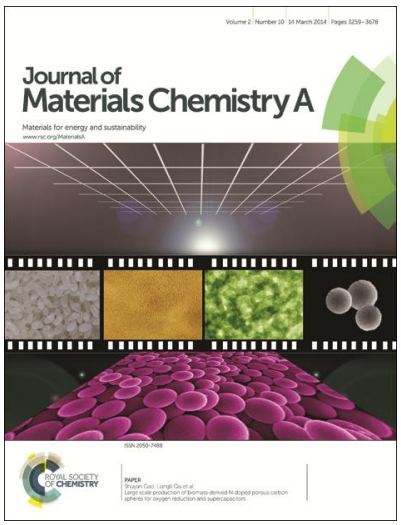

Journal of Materials Chemistry A

Materials for Energy and Sustainability

Full paper submission

Journal of Materials Chemistry A is a weekly journal in the materials field. The journal is interdisciplinary, publishing work of international significance on all aspects of materials chemistry related to energy and sustainability. Articles cover the fabrication, properties and applications of materials.

2012 Impact Factor of *Journal of Materials Chemistry*: **6.10**
For more information go to www.rsc.org/materialsA

The following paper has been submitted to *Journal of Materials Chemistry A* for consideration as a **full paper**.

Journal of Materials Chemistry A wishes to publish original research that demonstrates **novelty and advance**, either in the chemistry used to produce materials or in the properties/applications of the materials produced. Work submitted that is outside of these criteria will not usually be considered for publication. The materials should also be related to the theme of materials for energy and sustainability.

Routine or incremental work, however competently researched and reported, should not be recommended for publication if it does not meet our expectations with regard to novelty and impact.

It is the responsibility of authors to provide fully convincing evidence for the homogeneity and identity of all compounds they claim as new. Evidence of both purity and identity is required to establish that the properties and constants reported are those of the compound with the new structure claimed.

Thank you for your effort in reviewing this submission. It is only through the continued service of referees that we can maintain both the high quality of the publication and the rapid response times to authors. We would greatly appreciate if you could review this paper in **two weeks**. Please let us know if that will not be possible.

Once again, we appreciate your time in serving as a reviewer. To acknowledge this, the Royal Society of Chemistry offers a **25% discount** on its books: http://www.rsc.org/Shop/books/discounts.asp. Please also consider submitting your next manuscript to *Journal of Materials Chemistry A*.

Best wishes,

Liz Dunn
Managing Editor, *Journal of Materials Chemistry A*

Response to Reviews

For referee: 1

Comment: *There are minor queries which authors should address in the final resubmitted manuscript before it is accepted. The queries are:*

1. ***The life cycle studies carried out by authors reveal that there is degradation in current or electrochemical activity by 13.5 to 21 % after 1500 cycles which is quite disappointing. Generally any electrochromic device should have stability upto 10^6 cycles. So 1500 cycles is not a good response. Authors should improve the life cycle stability by limiting the oxidation potential to 0.4 to 0.6 V and study its electrochemical stability.***

   Response: Thanks for the referee's suggestion. We have supplemented the cycling stability of EC devices based on WO_3/PANI and NiO/PANI films measured at a low oxidation potential of 0.6 V (as shown in the Figure below) and added to the supporting information. The degradations of the peak currents at 0.6 V after 2000 cycles for the WO_3/PANI and NiO/PANI-3 films based on EC devices are 6% and 9.3%, respectively. Obviously, the cycle stability of the EC devices assembled by WO_3/PANI and NiO/PANI-3 films is highly enhanced when a low oxidation potential was applied. However, the result is still much lower than the value of 10^6 cycles. There are many factors affecting the cycle stability of the EC devices, including the chemical stability of the EC materials and electrolyte, the voltage window, the packaging technology of the devices and so on. We believe that the shorter lifetime of the EC devices assembled by WO_3/PANI and NiO/PANI-3 films is probably relate to the adhesion between films and substrate, the degradation of the PANI and the chemical instability of WO_3 and NiO in the electrolyte solution for a prolonged time, the electrolyte leakage (relate to the sealing property of the EC devices) and so on. Thus, it is necessary to improve the cycle stability by solving these problems in our next work.

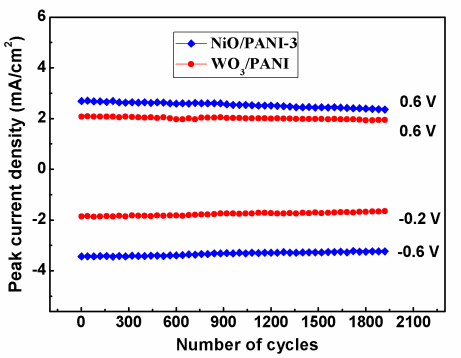

2. ***When we talk doping in conducting polymer polyaniline, we always refer to electrical conductivity. When polyaniline is doped with H_2SO_4, insertion of protons and conduction mechanism is different than if CLO_4^- are incorporated. Moreover protons play a dominant role in PANI rather than Li^+ ions. If PANI film is synthesized in H_2SO_4 medium then sulfate ions have to be removed from the polymer matrix before the film response is taken in $LiClO_4$ in PC. Even the CV response in non aqueous medium will be different than in aqueous H_2SO_4 medium. This is the reason why polyaniline films can't be grown in non-aqueous medium containing $LiClO_4$ medium. I will advise to carry out experiments of PANI growth in non aqueous medium and compare the data with PANI grown in H_2SO_4 medium. Even if the PANI film is grown in H_2SO_4 medium, after undoping and if we study the CV behavior in non-aqueous medium, cyclic voltammetric behavior will be different. So please be clear about the doping level in PANI film in H_2SO_4 medium and PANI doped with ClO_4^-***

Response: Thanks for your kindly advice. We have learned a lot from your comments, which have guiding significance for our future research. Although the PANI films were grown in H_2SO_4 medium in our present work, outstanding electrochromic properties were obtained in $LiClO_4$ in PC. Similar work has also been reported in the previous literature, where the PANI films grown in H_2SO_4 medium and the tests were performed in 1 M $LiClO_4$/PC medium (*Nanotechnology* 2008, 19, 465701). However, the influences of electrochemical performances have not been mentioned when the electrolyte changed from H_2SO_4 medium to $LiClO_4$ in PC. Just as the referee mentioned above, insertion of protons, conduction

mechanism and cyclic voltammetric behaviors will be different when the PANI were doped with H_2SO_4 and CLO_4^- (Even if the PANI film is undoped after grown in H_2SO_4 medium). Thus, it is necessary to carry out experiments of PANI growth in non aqueous medium and then compare the electrochemical and electrochromic performances with that of the PANI grown in H_2SO_4 medium. However, if we employ this new synthetic system, there will be a lot of experiments need to be done and this could not be completed during a short-term revision process. In this manuscript, we report high-quality metal oxide/conjugated polymer hierarchical nanoarrays grown directly on FTO-coated glass using a powerful two-step solution-based method. The highlight of this work is to improve the EC performances of the hybrid films through scrupulous design of the nanoarchitectures of the films making the organic and inorganic phases work synergistically during the electrochemical reactions. The current results can prove it. Therefore, we accept the referee's suggestion and a series of experiments will be carried out in our future work.

Cite this: DOI: 10.1039/c0xx00000x

www.rsc.org/xxxxxx

ARTICLE TYPE

Controllable Growth of High-Quality Metal Oxide/Conducting Polymer Hierarchical Nanoarrays with Outstanding Electrochromic Properties and Solar-Heat Shielding Ability

Dongyun Ma,[a,d] Guoying Shi,[c] Hongzhi Wang,*[a] Qinghong Zhang,[b] and Yaogang Li*[b]

Received (in XXX, XXX) Xth XXXXXXXXX 20XX, Accepted Xth XXXXXXXXX 20XX
DOI: 10.1039/b000000x

The high performance of organic/inorganic hybrid materials relies largely on a scrupulous design of nanoarchitectures so that the organic and inorganic phases can work synergistically. We present a powerful two-step solution-based method for the fabrication of hierarchical metal oxide/conducting polymer heterostructured nanoarrays. Demonstrated examples include different nanostructures (nanorod arrays, nanorod-based networks and nanoplate arrays) of metal oxides (WO_3 and NiO) and PANI (nanostubs, nanoparticales and nano-wrinkles). Given the unique composition and architecture, the hierarchical NiO/PANI nanoplate arrays show reversible multicolor changes, fast switching speeds of 90 and 120 ms for coloration and bleaching states, respectively, and superior coloration efficiency of 121.6 $cm^2\ C^{-1}$ under a low voltage of 1.2 V. Additionally, the application of the NiO/PANI nanoplate arrays coated FTO glass causes a temperature difference of 7~7.6 °C under different ambient temperatures, making it very attractive for potential applications in energy-saving smart windows. Our strategy paves the way for the design and synthesis of hierarchical metal oxide/conducting polymer nanoarrays with enhanced properties or new applications.

Introduction

Hybrid organic/inorganic materials with new functionalities have become one of the most active research areas of materials science.[1,2] Nanohybridization of a conducting polymer and a metal oxide semiconductor has been recognized as one of the most attractive combinations for the organic/inorganic hybrids.[3,4] They often combine the elasticity and functionality of the former and the high thermal and chemical stability followed by the strength of the latter, thereby endowing them to be effective candidates in various applications, such as photovoltaics,[5-8] electrochemical capacitors,[9,10] transistors and electrochromic (EC) devices.[11-13] An EC device is one of the most promising technological applications of metal oxides and conducting polymers.[14] Although promising EC performances such as electrochemically stable and excellent switching reversibility have been demonstrated with metal oxide nanostructures, the coloration efficiencies and switching responses still fall far behind that of conducting polymers.[13] Moreover, conducting polymer is a unique class of conjugated polymer with interesting optical properties due to its multiple redox states accompanied by rich color changes, while the metal oxides often undergo single color changes.[14] Therefore, synergistic combination of the merits of conducting polymers and metal oxides may provide an opportunity to develop a hybrid EC material with multicolor changing, high coloration efficiency, fast switching response and outstanding device lifetime.

In the past decade, there have been continuous attempts to combine conducting polymers with metal oxides to form nanostructured hybrid EC materials.[15-19] A wide variety of nanocomposites of conducting polymers with metal oxides have been reported, such as PANI/WO_3,[20-22] PEDOT/TiO_2,[23] Polypyrrole/WO_3,[24,25] and PANI/NiO,[26-28] where the organic and inorganic phases are held together by simple physical mixing. In this case, the interactions between the two phases are likely to be weak, because of the relatively small interfacial areas caused by oxide nanoparticles agglomeration.[29] Recently, covalently bonded PANI/TiO_2 and PANI/WO_3 hybrid thin films were fabricated using a sol-gel process or self-assembly technique to make interfacial interactions between the two components more prominent.[30,31] However, the hybrids showed compact structures, resulting in a relatively small surface area, which will influence the kinetics of coloration and bleaching processes that controlled by ion diffusion. Moreover, the inorganic material covalently bonded with conducting polymer has poor mechanical adhesion and electric connection with the supporting electrode, leading to slow transport of electrons into the EC layer to balance ions. All of these drawbacks and limitations cause the advantages of each individual component in the nanocomposites cannot be fully exerted, and thus further development is required.

In an effort to overcome the above mentioned obstacles, the main challenge is to design and realize a system with large interfacial area and strong interfacial interactions, in which the organic and inorganic phases can work synergistically. In this respect, the following two issues should be taken into account.

Firstly, with the hope of achieving a synergistic EC effect, the two components of the hybrid system should have a complementary or enhanced EC effect, such as WO_3/PANI or NiO/PANI. The former shows dual-electrochromism effect due to the non-overlapping of the coloration and bleaching between PANI and WO_3, while a superimposed EC effect can be achieved for the latter because the NiO and PANI possess synchronous coloration and bleaching voltages.[32,33] Secondly, the interconversion rate of conducting polymers between redox states is often limited by the slow transport of counter ions into the EC layer to balance charges, while the organized metal oxides nanostructures have a high surface-to-volume ratio and large tunnels for ion/electron intercalation processes.[34-36] Therefore, metal oxides can be served as host frameworks in the hybrid systems. By growing conducting polymers into such nanoarchitectures, hybrid assemblies with ordered structure and large interfacial area can be obtained. In such nanoscale configurations, both components have better electrical contact with the conductive substrate and will work synergistically.

In this article, we report a facile strategy for construction of hierarchical metal oxide/conducting polymer hybrid assemblies with adjustable components and heterostructures on FTO glass substrates. Demonstrated examples include different nanostructures (nanorod arrays, nanorod-based networks and nanoplate arrays) of metal oxides (WO_3 and NiO) and PANI (nanostubs, nanoparticales and nano-wrinkles) with a hierarchical and porous morphology. This unique architecture holds the merits of high surface area and short diffusion distances for easy electrolyte penetration, leading to more efficient ion/electron transports, and thus the superior EC performances were expected. Additionally, a comparative study of the energy-saving effect of hierarchical nanocomposites coated FTO glass and non-coated FTO glass was also conducted with a model house. This is the first model house used for the practical evaluation of the solar-heat shielding ability of EC smart windows.

Results and Discussion

We first present that the hierarchical WO_3/PANI hybrid can be obtained using a combined hydrothermal process and electrochemical polymerization. It is worth noting that the morphologies of PANI were varied with the electropolymerization procedures (Fig. S1). Fig. 1 illustrates the growth of WO_3/PANI nanoarrays on FTO glass substrates. The first step is to prepare WO_3 nanorods array backbone by hydrothermal method. Then PANI is directly assembled on the WO_3 nanorod surface by electrochemical polymerization.

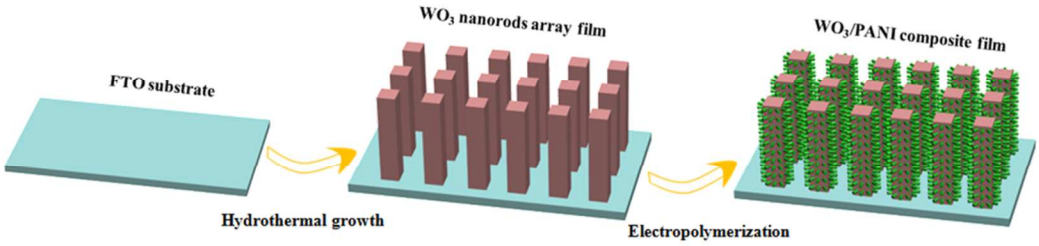

Fig. 1 Schematics of the fabrication of WO_3/PANI nanoarrays; the first step is to prepare WO_3 nanorods array backbone by hydrothermal method. Then PANI is directly assembled on the WO_3 nanorod surface by electrochemical polymerization.

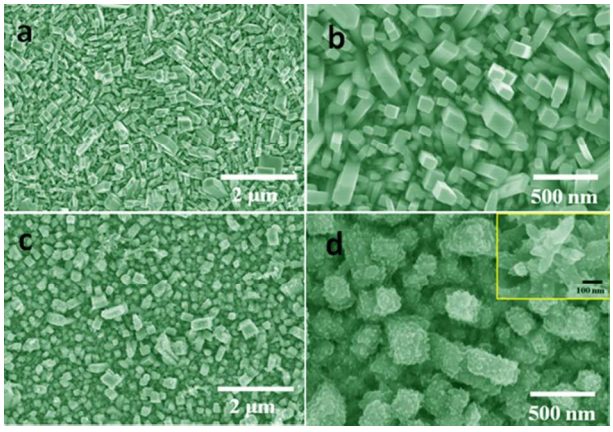

Fig. 2 (a,b) FESEM images of WO_3 nanorods array; (c,d) FESEM images of WO_3/PANI nanoarrays with a partial enlarged view in inset of (d).

The crystalline WO_3 film is composed of well-aligned rectangular WO_3 nanorods with a square cross-section of 80~120 nm (Fig. 2a,b). This unique nanostructure produces a coarse surface, which gives a larger surface area for the polymerization of PANI in the electrochemical processes. After carefully optimized potential cycling protocol at a scan rate of 100 mVs^{-1} for 100 cycles between -0.6 and 1.2 V, a thin PANI film is uniformly coated on each individual WO_3 nanorod, forming hierarchical WO_3/PANI nanoarrays (Fig. 2c,d). It can be seen from the inset of Fig. 2d that PANI film has nanostub-like morphology, which makes the surface of hybrid WO_3/PANI nanorods much rougher than the bare WO_3 nanorods and simultaneously the porous structure is well preserved.

The XRD patterns (Fig. 3a) reveal the crystalline WO_3 phase (hexagonal, JCPDS 85-2460) after electropolymerization; no obvious diffraction peaks of PANI are observed (Fig. S2), and therefore we conducted FTIR (Fig. 3b) measurement to further check the components of the WO_3/PANI nanoarrays. For bare WO_3 nanorod, the strong peaks centered at 920 cm^{-1} (contributed from stretching vibrations of W=O bonds), 874, 830, and 764 cm^{-1} (corresponding to the stretching vibrations of O-W-O bonds) are observed.[37] For the WO_3/PANI nanoarrays, in addition to the peaks of WO_3 several characteristic peaks of PANI are noticed. Two bands at 1564 and 1496 cm^{-1} are due to the C=C stretching vibrations of quinoid ring and benzenoid ring (quinoid ring and benzenoid ring are the basic molecular units of PANI), respectively. The bands at 1295 and 1212 cm^{-1} belong to the C−N and C=N stretching mode, respectively.[38,39] In comparison with the FTIR spectra of pure PANI and WO_3, redshifts of the bands

corresponding to the stretching vibrations of O-W-O bonds (from 874 to 868 cm^{-1}), C–N and C=N (from 1300 and 1243 cm^{-1} to 1295 and 1212 cm^{-1}, respectively) are found. This phenomenon indicates that the WO_3 phase is covalently bonded to PANI, which has been demonstrated in the previous literature.[31] Therefore, all results are in complete agreement in showing the formation of hybrid WO_3/PANI nanoarrays.

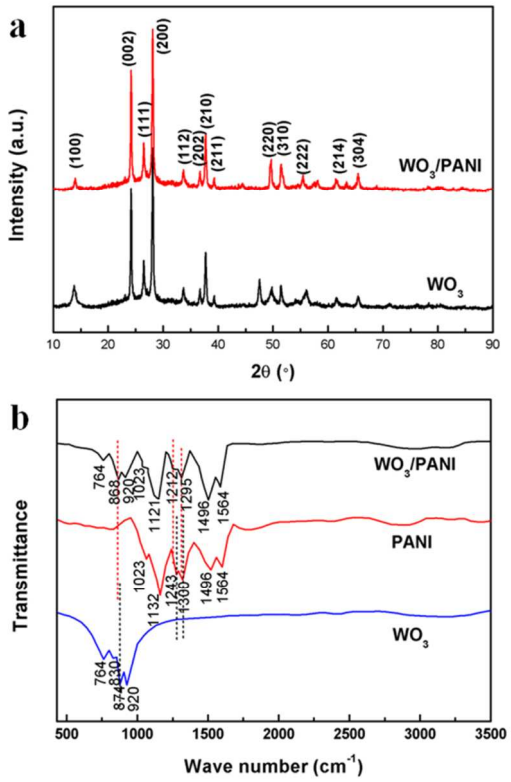

Fig. 3 (a) XRD patterns for both WO_3 and WO_3/PANI nanoarrays; (b) FTIR spectra of pure WO_3, PANI and hybrid WO_3/PANI nanoarrays.

Our strategy is powerful and general and can be easily extended to fabricate other metal oxide/conducting polymer hierarchical nanohybrids by simply choosing different metal oxide backbones (such as nanorod, nanoflake, and nanoplate) and conducting polymers. To demonstrate the versatility, we have also fabricated three distinct types of NiO/PANI nanoscale configurations. Fig. 4 shows the result of the first type of NiO/PANI nanostructure (NiO/PANI-1) grown on FTO glass via the similar polymer assembly on the NiO nano-network woven from nanorods. The nanorod diameter increases from 20 to 30 nm after homogeneous PANI nanoparticles growth, and the surface of hybrid NiO/PANI nanorods becomes much rougher than the bare NiO nanorods (Fig. 4c,d). Unfortunately, the PANI nanoparticles partially penetrated into the pores of NiO backbone during the electrodeposition process, which is not conducive to the ion migration, and therefore may affect the EC properties.

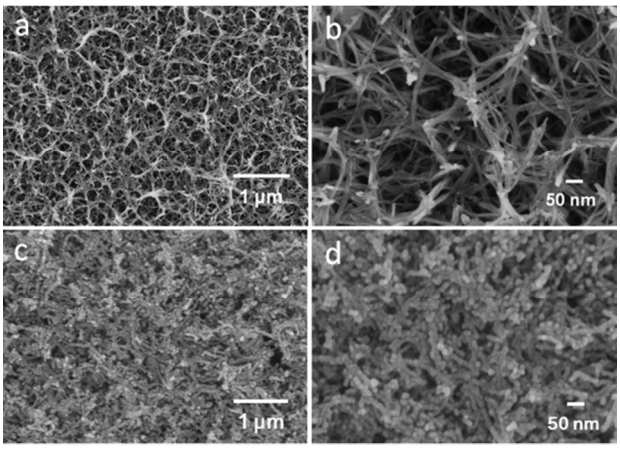

Fig. 4 (a, b) FESEM images of NiO nanorod-based networks; (c, d) FESEM images of the corresponding NiO/PANI nanohybrid composite.

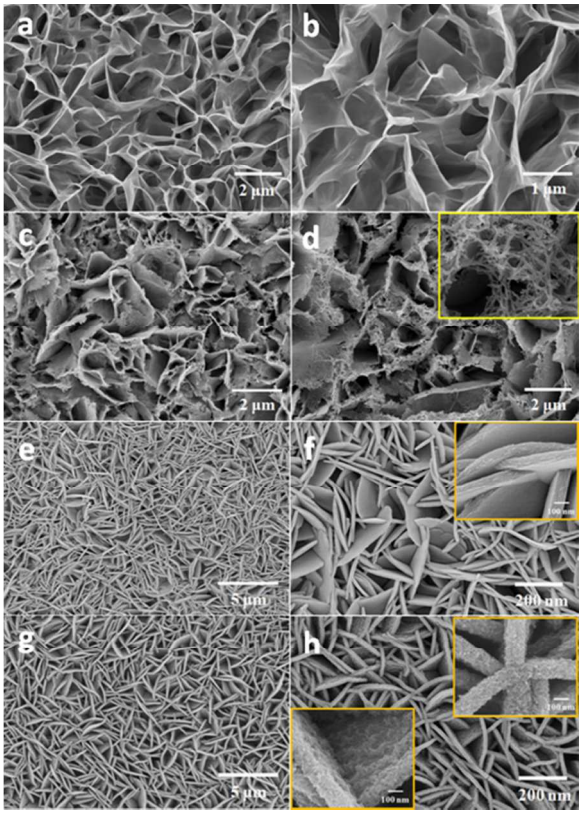

Fig. 5 (a, b) FESEM images of NiO nanoflakes and (c, d) the corresponding NiO/PANI nanohybrid composite; (e, f) FESEM images of NiO nanoplates array and (g, h) the corresponding NiO/PANI nanoarrays; the insets of (d), (f) and (h) show partial enlarged views.

For the second type of NiO/PANI nanostructure (NiO/PANI-2), a porous NiO nanoflake array is selected as the backbone for the subsequent electrodeposition of PANI nanostructure (Fig. 5a-d). Unlike the first type, PANI nanorod-based networks are grown on the top surface of NiO nanoflake (with a thickness of less than 10 nm and a width of about 2 to 3 μm) array. This is because both the NiO nanoflakes and open-pore voids between the nanoflakes are much larger than that of other NiO and WO_3 backbones in this work, and provide enough spaces for the growth of PANI nanorod networks. It is similar to the growth of PANI directly on FTO substrates, where the PANI nanorod

networks are also grown (Fig. S1e and f). Fig. 5e-h shows the example of obtained NiO/PANI nanoplates array (NiO/PANI-3). The third type of NiO/PANI nanoscale configuration holds the advantages of both NiO/PANI-1 and NiO/PANI-2. Firstly, each individual NiO nanoplate is covered with uniform PANI nano-wrinkles (the nanoplate thickness increases from 80 to 100 nm) and gives a coarse surface, which produces a larger active surface available for reactions in electrochemical processes. Secondly, the PANI nano-wrinkles are coated on the surface of NiO nanoplates and thus the porous structure is well preserved.

The presence of PANI is also confirmed by the XRD patterns and FTIR spectra as shown in Fig. 6. From the XRD patterns, it is confirmed that the intensive diffraction peaks between 2θ ranges of 30–90° are indexed to a cubic NiO phase (JCPDS 04-0835, Fig. S3), while the two broad peaks present at ~20 and 25° are ascribed to the periodicity parallel and perpendicular to the polymer chain of PANI,[40] respectively, indicating the growth of crystalline PANI in the successive potential cycling protocol. From the FTIR spectra, it can be seen that the strong peaks centered at 472, 560 cm^{-1} (contributed from stretching vibrations of Ni-O bonds) are observed;[41] in addition to the peaks of NiO the characteristic peaks of PANI are noticed. The results above are in complete agreement in showing the formation of hybrid NiO/PANI nanohybrids. Taking all, it is concluded that the developed methodology is general and powerful for preparing various metal oxide/ conducting polymer nanoarchitecture with tunable heterostructures, components, and morphologies.

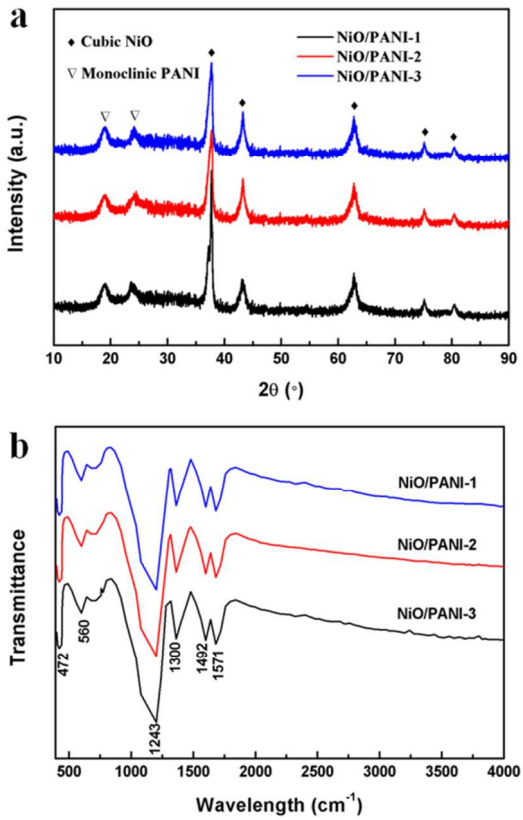

Fig. 6 (a) XRD patterns and (b) FTIR spectra for NiO/PANI-1, NiO/PANI-2 and NiO/PANI-3 nanohybrids, respectively.

In view of the unique compositions and architectures, the as-prepared WO_3/PANI and NiO/PANI nanohybrids are anticipated to display promising applications in EC devices. Characterizations of the electrochemical and EC properties of the WO_3/PANI nanorod arrays are provided in Fig. 7. The cyclic voltammetry (CV) curve of the WO_3/PANI nanrodarrays (Fig. 7a), as compared with those of pure WO_3 and PANI (Fig. S4), has typical redox peaks of PANI (c_1/a_1, c_2/a_2 and c_3/a_3) and WO_3 (c_4/a_4), which indicates that WO_3/PANI composite film is obtained successfully and it possesses activities of both PANI and WO_3. The redox couple c_4/a_4 is due to the WO_3-related redox process, involving the intercalation/deintercalation of Li^+ ions and electrons. The redox couples c_1/a_1 and c_3/a_3 correspond to the change between leucoemeraldine salt (LS) and emeraldine salt (ES), emeraldine salt (ES) and pernigraniline salt (PS) of PANI with anion doping/dedoping processes, respectively, simply expressed as follows:[22]

LS ⇌ ES:

$$\underset{\text{light yellow}}{PANI} + 2nClO_4^- \rightleftharpoons \underset{\text{green}}{(PANI^{2n+})(ClO_4^-)_{2n}} + 2ne^- \quad (1)$$

ES ⇌ PS:

$$\underset{\text{green}}{(PANI^{2n+})(ClO_4^-)_{2n}} + 2nClO_4^- \rightleftharpoons \underset{\text{blue}}{(PANI)^{4n+}(ClO_4^-)_{4n}} + 2ne^- \quad (2)$$

The redox couple c_2/a_2 can be ascribed to hydrolysis products of PANI due to over-oxidation at comparatively high potential.[42] The WO_3/PANI nanorod arrays show evident electrochromism with reversible multicolor changes under different applied potentials (inset of Fig. 7b) and the corresponding optical changes are recorded by the transmittance spectra (Fig. 7b). The optical modulation, *i.e.*, the transmittance variation of samples under different applied potentials, together with the switching speed and coloration efficiency are very important factors in practical applications of EC systems. For the WO_3/PANI nanorod arrays, the optical modulation is larger than that of pure PANI film (Fig. S5) and a maximum value of 42% is reached between -0.2 and 0.8 V at 632.8 nm. The chronoamperometry (by applying different potentials) and corresponding *in situ* transmittance measurements were employed to study the switching time characteristics of the samples. In this case, the switching times were defined as the time required for a 90% change in the whole transmittance modulation. Fig. 7c shows the dynamic switching times of the WO_3/PANI nanorod arrays under a square wave voltage between -0.2 and 0.8 V with a pulse width of 5 s. The response times under the voltages of -0.2 and 0.8 V are found to be 500 and 800 ms, respectively, faster than those of the inorganic EC films such as WO_3 and NiO (more than 2 s),[34-36,43] PANI/WO_3 dense film (9.9 s),[22] and WO_3 nanorod embedded PANI composite film (0.9 s).[44]

Coloration efficiency (CE), namely the change in the optical density (ΔOD) per unit charge density (Q/A) during switching, is one of the most important criteria for selecting an EC material, and can be calculated according to the following formulas:

$$CE = \Delta OD/(Q/A) \quad (3)$$

$$\Delta OD = \log(T_b/T_c) \quad (4)$$

where T_b and T_c refer to the transmittances of the film in its bleached and colored states, respectively. Fig. 7d shows plots of the *in situ* ΔOD at 632.8 nm *versus* intercalation charge density (applying a voltage of 0.8 V) for the WO_3/PANI nanorod arrays. The CE is extracted as the slope of the line fitting the linear region of the curve. The calculated CE value of the WO_3/PANI nanorod arrays is 76 cm^2 C^{-1}. This value is much higher than that of pure PANI film (Fig. S6) (49.2 cm^2 C^{-1}), and shows an improvement of approximately 55%.

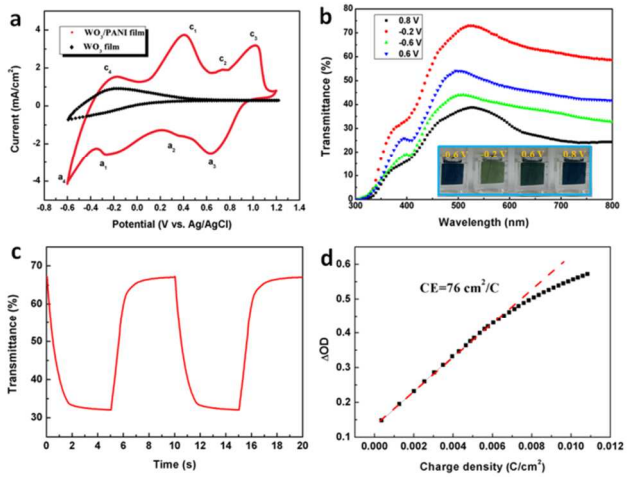

Fig. 7 (a) Cyclic voltammetry curves of pure WO_3 and WO_3/PANI nanoarrays measured in 1.0 M lithium perchlorate–PC solution with a sweep rate of 20 mV/s between -0.6 and 1.2 V; (b) transmittance spectra of WO_3/PANI nanoarrays under different voltages, with inset showing the digital photos of WO_3/PANI nanoarrays under different voltages; (c) Switching time characteristics for WO_3/PANI nanoarrays measured at 632.8 nm between -0.2 and 0.8 V; (d) ΔOD variation with respect to the charge density for WO_3/PANI nanoarrays.

In comparison with the WO_3/PANI nanorod arrays, which shows dual-electrochromism effect due to the non-overlapping of the coloration and bleaching between PANI and WO_3, a superimposed EC effect can be achieved for NiO/PANI hybrids because both the NiO and PANI show colored states at positive potentials and bleached states at negative potentials, respectively. Similarly, the NiO/PANI nanohybrids show evident electrochromism with reversible multicolor changes under different applied potentials (Fig. 8d). According to the above definitions, characterizations of the optical modulation, switching times and CE for the three types of NiO/PANI nanohybrids were conducted under different voltages with a pulse width of 5 s. Fig. 8a-c shows the transmittance spectra of NiO/PANI-1, NiO/PANI-2 and NiO/PANI-3 nanohybrids under different voltages, respectively. As the applied potential increases from -0.6 to 1.2 V, the transmittance of the sample decreases sharply and thus large optical modulations of 50%, 38% and 62% are reached for NiO/PANI-1, NiO/PANI-2 and NiO/PANI-3 nanohybrids between -0.6 and 1.2 V at 550 nm, respectively. The maximum value of 62% is larger than those of NiO/PANI dense film (31%)[45] and porous NiO/PANI composite film (56%).[27]

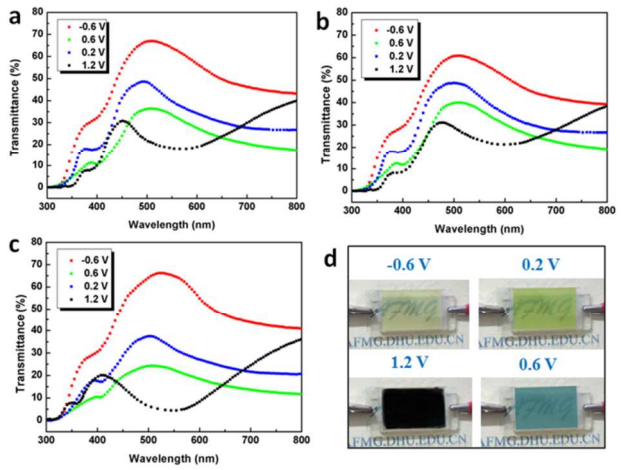

Fig. 8 (a-c) Transmittance spectra for NiO/PANI-1, NiO/PANI-2 and NiO/PANI-3 nanohybrids under different voltages, respectively; (d) digital photos of NiO/PANI-3 under different voltages.

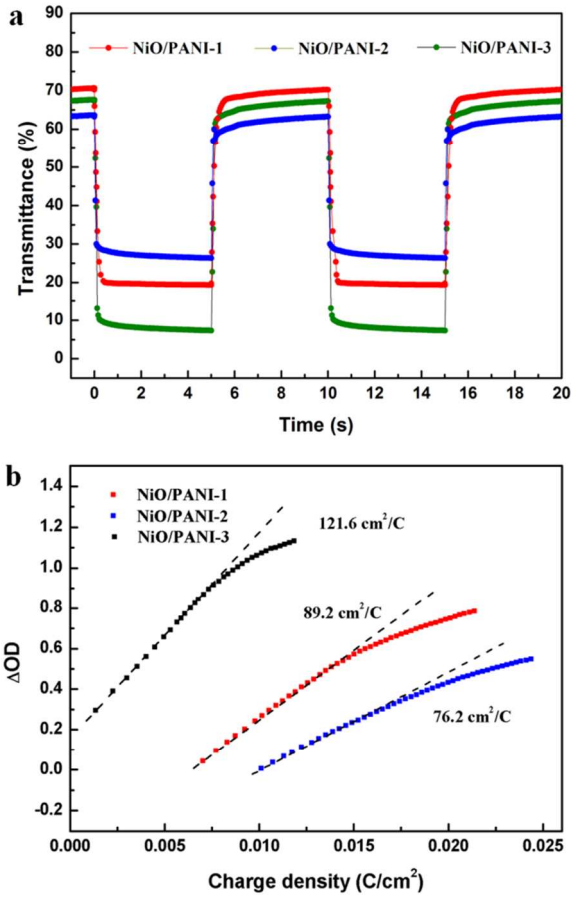

Fig. 9 (a) Switching time characteristics for NiO/PANI nanohybrids measured at 632.8 nm between -0.6 and 1.2 V; (d) ΔOD variation with respect to the charge density for NiO/PANI nanohybrids.

Table 1 Summary of the response times for the NiO/PANI hybrid films

Sample	Coloration times (1.2 V)	Bleaching times (-0.6 V)
NiO/PANI-1	384 ms	629 ms
NiO/PANI-2	63 ms	86 ms
NiO/PANI-3	90 ms	120 ms

The switching times of samples are calculated from Fig. 9a and summarized in Table 1. Obviously, the NiO/PANI-2 and NiO/PANI-3 show faster response speeds than NiO/PANI-1. The reason is that PANI nanoparticles partially penetrated into the pores of NiO backbone during the electrodeposition process, which may hinder the ion migration rate. Fig. 9b shows plots of the *in situ* ΔOD at 550 nm *versus* intercalation charge density (applying a voltage of 1.2 V) for the NiO/PANI nanohybrids. As described in the previous section, the NiO/PANI-3 holds the advantages of both NiO/PANI-1 and NiO/PANI-2. Thus, a high CE value of 121.6 cm^2 C^{-1} is achieved for the NiO/PANI-3. This value is much higher than that of the NiO/PANI-1 and NiO/PANI-2 (89.2 and 76.2 cm^2 C^{-1}, respectively), and shows an improvement of approximately 36-60%.

The noticeable EC performance of the hierarchical WO_3/PANI and NiO/PANI nanohybrids can be mainly attributed to the unique nanoarrays architecture. On one hand, the WO_3 nanorod arrays and NiO nanoplate arrays with good adhesion to FTO substrates provide not only a stable mechanical support for the active PANI but also a template for homogeneous coverage of PANI, leading to large interfacial area and strong interfacial interactions, where the organic and inorganic phases can work synergistically. In addition, the large interfacial area will enhance the inter charge transfer and thus large optical contrast and fast switching speed can be achieved. On the other hand, the highly porous structure has a high surface-to-volume ratio that favors an efficient contact between active materials and the electrolyte. Meanwhile, the large tunnels formed by the ordered WO_3 and NiO nanostructures lead to a large diffusion coefficient, and reduce the diffusion path lengths for both electrons and ions, thus leading to fast switching kinetics.

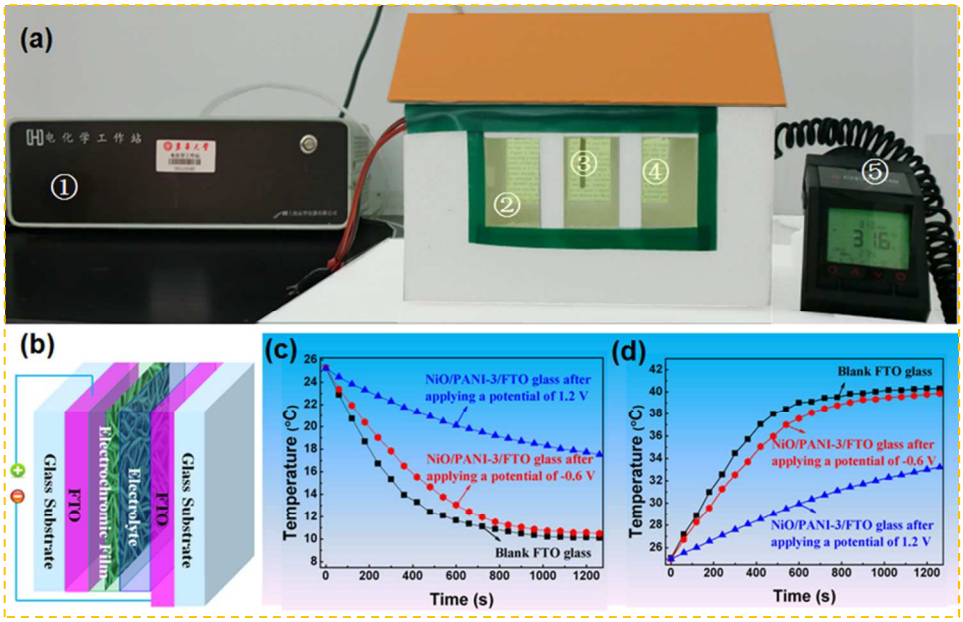

Fig. 10 (a) Photographic illustration of the testing system, 1: electrochemical workstation, 2 and 4: test windows installed in the front and back of the room, respectively, 3: temperature probe, and 5: portable thermometer; (b) scheme of the test windows; (c) and (d) temperature dependence on time for NiO/PANI-3 coated FTO glass with the temperature of thermostatic chamber fixed at 10 and 40 °C, respectively.

The EC devices can be used in energy-saving smart windows to tune the indoor light and temperature. In this work, we have constructed a model house (Fig. 10a) to evaluate the solar-heat shielding ability of WO_3/PANI and NiO/PANI hybrids coated FTO glass; the results are shown in Fig. 10 and Supporting Information. The house was made of boards (thermal conductivity k=0.026 $Wm^{-1}K^{-1}$) with a thickness of 2.0 cm and the inner space had a volume of 1.8×10^3 cm^3 ($22\times8\times10$ cm^3). Six coated or non-coated FTO glasses were installed in the front and back of the room, respectively, and the space was sealed during the testing process. The experiment was performed at a thermostatic chamber and the temperature was fixed at 40 or 10 °C, while the initial temperature of room was about 25 °C. A portable thermometer (laserSight LT, Optris, Germany) was employed to monitor the room temperature changes. The results (Fig. 10c) indicate that the application of the NiO/PANI-3 coated FTO glass causes a temperature difference of about 7.6 °C compared with the blank FTO glass, namely the inner room temperature can be maintained at 17.6 °C when the outer room (thermostatic chamber) temperature fix at 10 °C. In another case, the inner room temperature can be maintained at 33 °C when the outer room temperature fix at 40 °C, namely, a temperature reduction of about 7 °C is achieved. This property makes it possible to keep inner room cool in summer and warm in winter.

Conclusions

In summary, we have demonstrated the nanohybridization of metal oxide and conducting polymer can be achieved using a combined hydrothermal process and electrochemical polymerization. Detailed experimental results reveal that PANI (nanostubs, nanoparticales and nano-wrinkles) can directly assemble on different metal oxide nanostructures including WO_3 nanorod arrays and NiO nanorod networks, nanoflakes or nanoplate arrays. The morphology of PANI is dependent on the electropolymerization procedures (potentio-, galvanostatic and potential cycling protocols). Because of their unique composition

and architecture, the hierarchical NiO/PANI nanoplate arrays show reversible multicolor changes, fast switching speed of 90 and 120 ms for coloration and bleaching states, respectively, and superior coloration efficiency of 121.6 cm^2 C^{-1} under a low voltage of 1.2 V. Moreover, the application of the NiO/PANI nanoplate arrays coated FTO glass causes a temperature difference of 7~7.6 °C under different ambient temperatures, making it very attractive for potential applications in energy-saving smart windows. Additionally, our powerful and general method could enable the fabrication of other metal oxide/conducting polymer heteronanostructures for selected applications in optical coating, electrochemical energy storage, and optoelectronic devices.

Experimental Section

Preparation of WO_3 nanorod array and nanoporous NiO electrodes: Vertically aligned WO_3 nanorod arrays were grown on FTO coated glass substrates using a facile hydrothermal technique.[35] In a typical procedure, tungstenic acid (H_2WO_4) powder was dissolved in 30 wt% H_2O_2, while heating at 95 °C with stirring. The resulting solution was diluted using deionized water, giving a concentration of 0.1 M. The reaction solution for hydrothermal use was obtained by mixing 10.5 mL H_2WO_4 solution (0.1 M), 3.5 mL HCl (3 M) and 1.2 mmol urea in 24 mL deionized water, and then transferred to a 70 mL Teflon-lined stainless steel autoclave, holding a vertically oriented WO_3 seed layer coated FTO glass. The WO_3 seed layer was deposited on FTO glass by spin-coating a seed solution of 1.5 g H_2WO_4 in 10 mL 30 wt% H_2O_2, followed by annealing at 400 °C for 1 h. Finally, the autoclave was sealed and maintained at 180 °C for 12 h. The samples were rinsed with deionized water several times and dried at room temperature.

The porous NiO nanostructures were prepared by another facile hydrothermal synthesis method as follow. Before hydrothermal growth, a seed layer was deposited on FTO glass via spin-coating a seed solution made by adding 0.5 g of nickel acetate to 9 mL of a mixed solution of ethanol and n-butanol with a volume ratio of 1:2, followed by heating at 60 °C in a vacuum oven for 6 h.

There are many factors affecting the formation and crystal growth of hydrothermal products, including the capping agent, solvent system, and reaction time. In our experiments, we note that using the same synthesis technique three distinct types of NiO nanostructures were obtained by modification of the reaction solution composition. For the NiO nanorod-based networks, 0.6 g of nickel acetate and 0.6 g of urea were added into 56 mL of deionized water. The reaction was kept at 180 °C for 6 h and then annealed at 400 °C for 2 h. For the NiO nanoflake, 1.24 g of nickel acetate and 0.6 g of urea were added into 56 mL of absolute alcohol. The reaction was kept at 180 °C for 6 h and then annealed at 400 °C for 2 h. For the NiO nanoplate arrays, 0.6 g of nickel acetate, 0.3 g of potassium persulfate and 3mL condensed aqueous ammonia were added into 53 mL of deionized water. The reaction was kept at 180 °C for 6 h and then annealed at 400 °C for 2 h.

Electrosynthesis of WO_3/PANI and NiO/PANI hierarchical hybrids: After a series of tentative experiments, the potentiodynamic methods were prove to be more appropriate for the deposition of PANI on the above WO_3 and NiO nanostructures than potentio- and galvanostatic procedures. Electrolyte for electro-polymerization of PANI was obtained by dissolving 0.93 g of aniline into 200 mL of 0.5 M H_2SO_4 solution. The polymerization of aniline was carried out by a simple, but carefully optimized potential cycling protocol at a scan rate of 100 mVs^{-1} for 100 cycles between -0.6 and 1.2 V, where the above WO_3 nanorod array and nanoporous NiO electrodes as the working electrode, Ag/AgCl as the reference electrode and a Pt foil as the counter electrode. Finally, the samples were rinsed with deionized water and absolute alcohol, followed by heating at 60 °C in a vacuum oven for 6 h.

Characterization techniques: The morphology and microstructure of the samples were characterized by X-ray diffraction (XRD, D/max 2550 V, Rigaku, Japan, Cu Ka (λ=0.154 nm) radiation at 40 kV and 200 mA in the 2θ range of 10–90°), field emission scanning electron microscopy (FESEM, Hitachi, S-4800). The FTIR spectra were recorded on a Nicolet NEXUS-670 spectrometer from 500 to 3500 cm^{-1}. The *in situ* transmission spectra of the as-prepared electrodes in the colored and bleached states were measured over the range from 300 to 800 nm using a UV-vis spectrophotometer (Lambda 950, Perkin Elmer, Waltham, MA, USA).

Electrochemical and Electrochromic Measurements: The cyclic voltammetry (CV) measurements were carried out on an electrochemical workstation (CHI760D, Shanghai Chenhua Instruments, China) using a three-electrode test cell, which consisted of the working electrode (WO_3, NiO, WO_3/PANI or NiO/PANI), a platinum wire counter electrode, and a Ag/AgCl reference electrode in the electrolyte of 1.0 M lithium perchlorate ($LiClO_4$) in propylene carbonate (PC). The coloration/bleaching switching characteristics were recorded *in situ* using a UV-vis spectrophotometer with an absorbance wavelength of 632.8 and 550 nm for WO_3/PANI and NiO/PANI electrodes, respectively. The chronoamperometry tests were performed on the electrochemical workstation under different squarewave voltages with a pulse width of 5 s.

Energy-saving Effect Evaluation: The solar-heat shielding ability of WO_3/PANI and NiO/PANI hybrids coated FTO glass was conducted with a model house. The house was made of boards (thermal conductivity k=0.026 $Wm^{-1}K^{-1}$) with a thickness of 2.0 cm and the inner space had a volume of 1.8×10^3 cm^3 ($22\times8\times10$ cm^3). Six coated or non-coated FTO glasses were installed in the front and back of the room, respectively, and the space was sealed during the testing process. The experiment was performed at a thermostatic chamber and the temperature was fixed at 40 or 10 °C, while the initial temperature of room was about 25 °C. A portable thermometer (laserSight LT, Optris, Germany) was employed to monitor the room temperature changes.

Acknowledgements

We gratefully acknowledge the financial support by Natural Science Foundation of China (No. 51172042), Specialized Research Fund for the Doctoral Program of Higher Education (20110075130001), Science and Technology Commission of Shanghai Municipality (12nm0503900,13JC1400200), the Program for Professor of Special Appointment (Eastern Scholar) at Shanghai Institutions of Higher Learning, Innovative Research

Team in University (IRT1221) and the Program of Introducing Talents of Discipline to Universities (No.111-2-04).

Notes and references

[a] *State Key Laboratory for Modification of Chemical Fibers and Polymer Materials, College of Materials Science and Engineering, Donghua University, Shanghai 201620, P. R. China. Fax: +86-021-67792855; Tel: +86-021-67792881; E-mail: wanghz@dhu.edu.cn*

[b] *Engineering Research Center of Advanced Glasses Manufacturing Technology, Ministry of Education, College of Materials Science and Engineering, Donghua University, Shanghai 201620, P. R. China. Fax: +86-021-67792855; Tel: +86-021-67792526; E-mail: yaogang_li@dhu.edu.cn*

[c] *College of Chemistry, Chemical Engineering and and Biotechnology, Donghua University, Shanghai 201620, China.*

[d] *School of Materials Science and Engineering, Shanghai University, Shanghai 200444, P. R. China.*

† Electronic Supplementary Information (ESI) available: [FESEM images of PANI films prepared using potentiostatic procedure, galvanostatic procedure and potentiodynamic cycle, respectively; XRD patterns of porous NiO films prepared by facile hydrothermal synthesis method; Cyclic voltammetry curves of PANI films deposited by potentiostatic, galvanostatic procedures and potentiodynamic cycle, respectively; Transmittance spectra of PANI films and the corresponding digital photos of PANI films under different voltages; Switching time characteristics measured at 632.8 nm between -0.6 and 0.8 V and ΔOD variation with respect to the charge density for the PANI films prepared by potentiodynamic cycle; Temperature dependence on time for NiO/PANI -1, NiO/PANI -2 and WO_3/PANI coated FTO glasses with the temperature of thermostatic chamber fixed at 10 and 40 °C, respectively; Peak current evolution of the WO_3/PANI and NiO/PANI-3 films during the step chronoamperometric cycles.]. See DOI: 10.1039/b000000x/

1 C. Sanchez, P. Belleville, M. Popalld and L. Nicole, *Chem. Soc. Rev.,* 2011, **40**, 696.
2 M. J. Buehler, P. Rabu and A. Taubert, *Eur. J. Inorg. Chem.,* 2012, **32**, 5092.
3 G. H. Yu, X. Xie, L. J. Pan, Z. N. Bao and Y. Cui, *Nano Energy,* 2013, **2**, 213.
4 P. J. Hagrman, D. Hagrman and J. Zubieta, *Angew. Chem. Int. Ed.,* 1999, **38**, 2638.
5 M. Wright and A. Uddin, *Sol. Energy Mater. Sol. Cells,* 2012, **107**, 87.
6 S. D. Oosterhout, M. M. Wienk, S. S. van Bavel, R. Thiedmann, L. J. A. Koster, J. Gilot, J. Loos, V. Schmidt and R. A. J. Janssen, *Nat. Mater.,* 2009, **8**, 818.
7 W. R. Wei, M. L. Tsai, S. T. Ho, S. H. Tai, C. R. Ho, S. H. Tsai, C. W. Liu, R. J. Chung and J. H. He, *Nano Lett.,* 2013, **13**, 3658.
8 J. H. Heo, S. H. Im, J. H. Noh, T. N. Mandal, C. S. Lim, J. A. Chang, Y. H. Lee, H. J. Kim, A. Sarkar, M. K. Nazeeruddin, M. Grätzel and S. I. Seok, *Nat. Photonics,* 2013, **7**, 486.
9 L. Chen, Z. X. Song, G. C. Liu, J. S. Qiu, C.Yu, J. W. Qin, L. Ma, F. Q. Tian and W. Liu, *J. Phys. Chem. Solids,* 2013, **74**, 360.
10 K. R. Prasada and N. Miura, *Electrochem. Solid-State Lett.,* 2004, **7**, A425.
11 F. D. Franco, P. Bocchetta, C. Cali, M. Mosca, M. Santamaria and F. D. Quarto, *J. Electrochem. Soc.,* 2010, **158**, H50.
12 M. S. Hammer, C. Deibel, J. Pflaum and V. Dyakonov, *Org. Electron.,* 2010, **11**, 1569.
13 V. K. Thakur, G. Q. Ding, J. Ma, P. S. Lee and X. H. Lu, *Adv. Mater.,* 2012, **24**, 4071.
14 P. M. S. Monk, R. J. Mortimer and D. R. Rosseinsky, *Electrochromism and Electrochromic Devices*, Cambridge, New York 2007.
15 W. Caseri, *J. Mater. Chem.,* 2010, **20**, 5582.
16 C. M. Amb, P. M. Beaujuge and J. R. Reynolds, *Adv. Mater.,* 2010, **22**, 724.
17 T. T. Steekler, X. Zhang, J. Hwang, R. Honeyager, S. Ohira, X. H. Zhang, A. Grant, S. Ellinger, S. A. Odom, D. Sweat, D. B. Tanner, A. G. Rinzler, S. Barlow, J. L. Bredas, B. Kippelen, S. R. Marder and J. R. Reynolds, *J. Am. Chem. Soc.,* 2009, **131**, 2824.
18 S. Takagi, S. Makuta, A. Veamatahau, Y. Otsuka and Y. Tachibana, *J. Mater. Chem.,* 2012, **22**, 22181.
19 X. H. Xia, D. L.Chao, X. Y. Qi, Q. Q. Xiong, Y. Q. Zhang, J. P. Tu, H. Zhang and H. J. Fan, *Nano Lett.,* 2013, **13**, 4562.
20 P. K. Shen, H. T. Huang and A. C. C. Tseung, *J. Electrochem. Soc.,* 1992, **139**, 1840.
21 J. H. Zhu, S. Y. Wei, L. Zhang, Y. B. Mao, J. Ryu, A. B. Karki, D. P. Younge and Z. H. Guo, *J. Mater. Chem.,* 2011, **21**, 342.
22 H. G. Wei, X. R. Yan, S. J. Wu, Z. P. Luo, S. Y. Wei and Z. H. Guo, *J. Phys. Chem. C,* 2012, **116**, 25052.
23 L. J. Ma, Y. X. Li, X. F. Yu, Q. B. Yang and C. H. Noh, *Sol. EnergyMater. Sol. Cells,* 2008, **92**, 1253.
24 J. H. Zhu, S. Y. Wei, L. Zhang, Y. B. Mao, J. Ryu, P. Mavinakuli, A. B. Karki, D. P. Young and Z. H. Guo, *J. Phys. Chem. C,* 2010, **114**, 16335.
25 D. S. Lee, D. D. Lee, H. R. Hwang, J. H. Paik and J. S. Huh, *J. Mater. Sci.,* 2001, **12**, 41.
26 F. Svegl, A. S. Vuk, M. Hajzeri, L. S. Perse and B. Orel, *Sol. Energy Mater. Sol. Cells,* 2012, **99**, 14.
27 X. H. Xia, J. P. Tu, J. Zhang, X. L. Wang, W. K. Zhang and H. Huang, *Nanotechnology,* 2008, **19**, 465701.
28 M.Aleahmad, H. G.Taleghani and H. Eisazadeh, *Synth. Met.,* 2011, **161**, 990.
29 C. Janáky, N. R. de Tacconi, W. Chanmanee and K. Rajeshwar, *J. Phys. Chem. C,* 2012, **116**, 19145.
30 S. X. Xiong, S. L. Phua, B. S. Dunn, J. Ma and X. H. Lu, *Chem. Mater.,* 2010, **22**, 255.
31 J. Zhang, J. P. Tu, D. Zhang, Y. Q. Qiao, X. H. Xia, X. L. Wang and C. D. Gu, *J. Mater. Chem.,* 2011, **21**, 17316.
32 G. A. Niklasson and C. G. Granqvist, *J. Mater. Chem.,* 2007, **17**, 127.
33 G. F. Cai, J. P. Tu, D. Zhou, J. H. Zhang, X. L.Wang and C. D. Gu, *Sol. Energy Mater. Sol. Cells,* 2014, **122**, 51.
34 D. Y. Ma, H. Z. Wang, Q. H. Zhang and Y. G. Li, *J. Mater. Chem.,* 2012, **22**, 16633.
35 D. Y. Ma, G. Y. Shi, H. Z. Wang, Q. H. Zhang and Y. G. Li, *J. Mater. Chem. A,* 2013, **1**, 684.
36 D. Y. Ma, G. Y. Shi, H. Z. Wang, Q. H. Zhang and Y. G. Li, *Nanoscale,* 2013, **5**, 4808.
37 C. G. Granqvist, *Sol. Energy Mater. Sol. Cells,* 2000, **60**, 201.
38 A. Kellenberger, E. Dmitrieva and L. Dunsch, *J. Phys. Chem. B,* 2012, **116**, 4377.
39 W. A. El-Said, C. H. Yea, J. W. Choi and I. K. Kwon, *Thin Solid Films,* 2009, **518**, 661.
40 G. P. Song, J. Han and R. Guo, *Synth. Met.,* 2007, **157**, 170.
41 X. H. Xia, J. P. Tu, X. H. Xia, X. L. Wang and J. Y. Xiang, *Electrochem. Comm.,* 2008, **10**, 1288.
42 H. V. Hoang and R. Holze, *Chem. Mater.,* **2006**, *18*, 1976.
43 J. Zhang, J. P. Tu, X. H. Xia, X. L. Wang and C. D. Gu, *J. Mater. Chem.,* 2011, **21**, 5492.
44 J. Zhang, J. P. Tu, G. H. Du, Z. M. Dong, Y. S. Wu, L. Chang, D. Xie, G. F. Cai and X. L. Wang, *Sol. Energy Mater. Sol. Cells,* 2013, **114**, 31.
45 A. C. Sonavane, A. I. Inamdar, H. P. Deshmukh and P. S. Patil, *J. Phys. D: Appl. Phys.,* 2010, **43**, 315102.

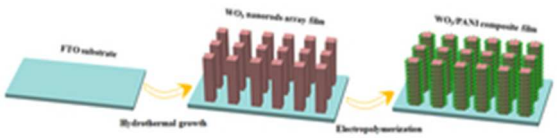

Fig. 1 Schematics of the fabrication of WO_3/PANI nanoarrays; the first step is to prepare WO_3 nanorods array backbone by hydrothermal method. Then PANI is directly assembled on the WO_3 nanorod surface by electrochemical polymerization.
23x5mm (300 x 300 DPI)

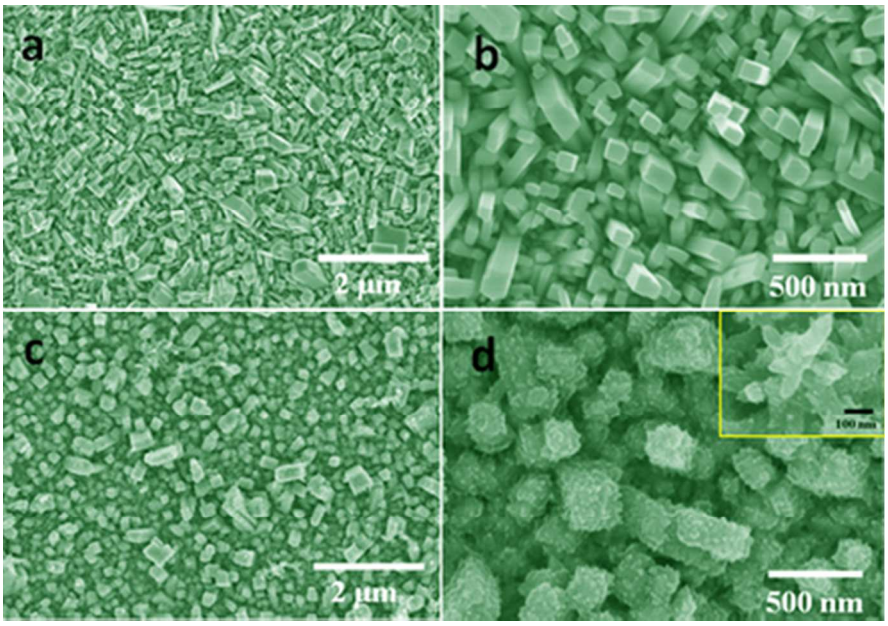

Fig. 2 (a,b) FESEM images of WO_3 nanorods array; (c,d) FESEM images of WO_3/PANI nanoarrays with a partial enlarged view in inset of (d).
37x25mm (300 x 300 DPI)

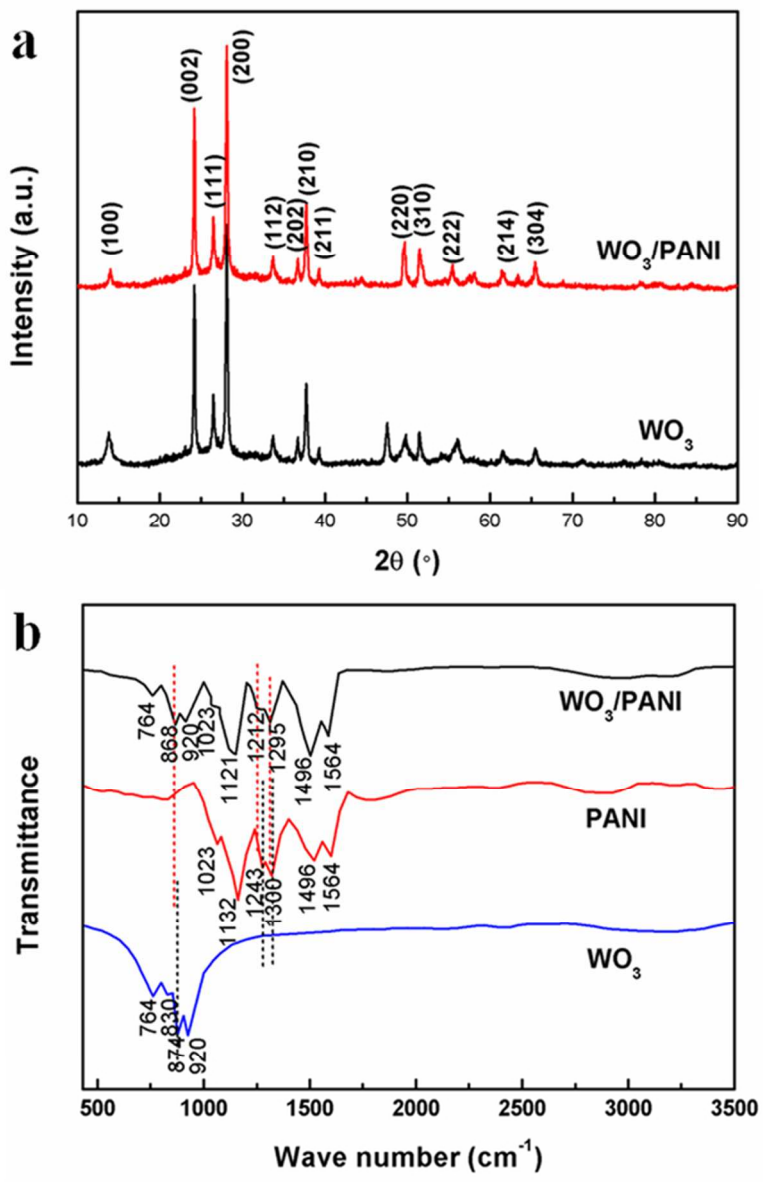

Fig. 3 (a) XRD patterns for both WO_3 and WO_3/PANI nanoarrays; (b) FTIR spectra of pure WO_3, PANI and hybrid WO_3/PANI nanoarrays.
53x80mm (300 x 300 DPI)

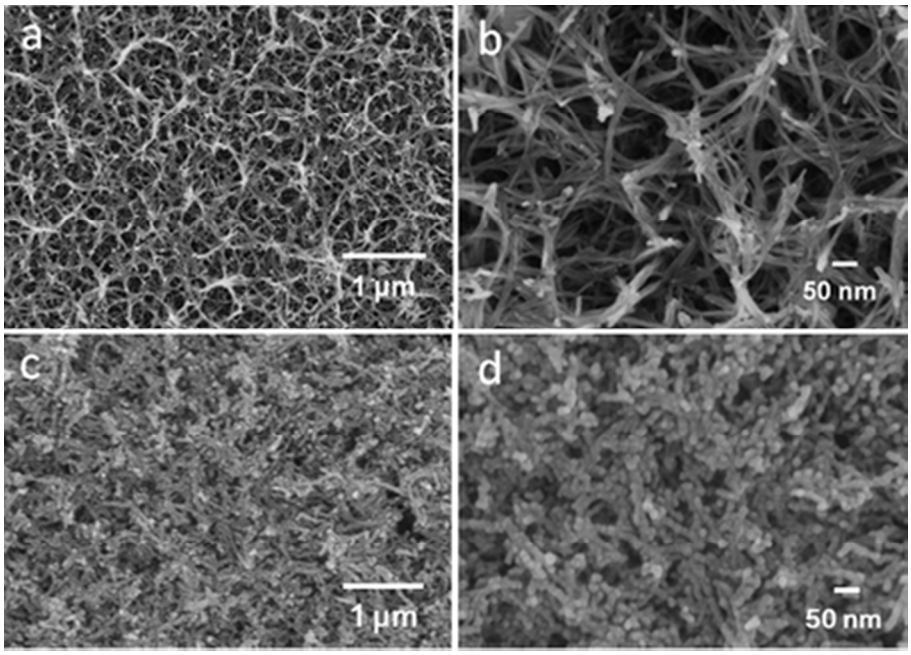

Fig. 4 (a, b) FESEM images of NiO nanorod-based networks; (c, d) FESEM images of the corresponding NiO/PANI nanohybrid composite.
38x27mm (300 x 300 DPI)

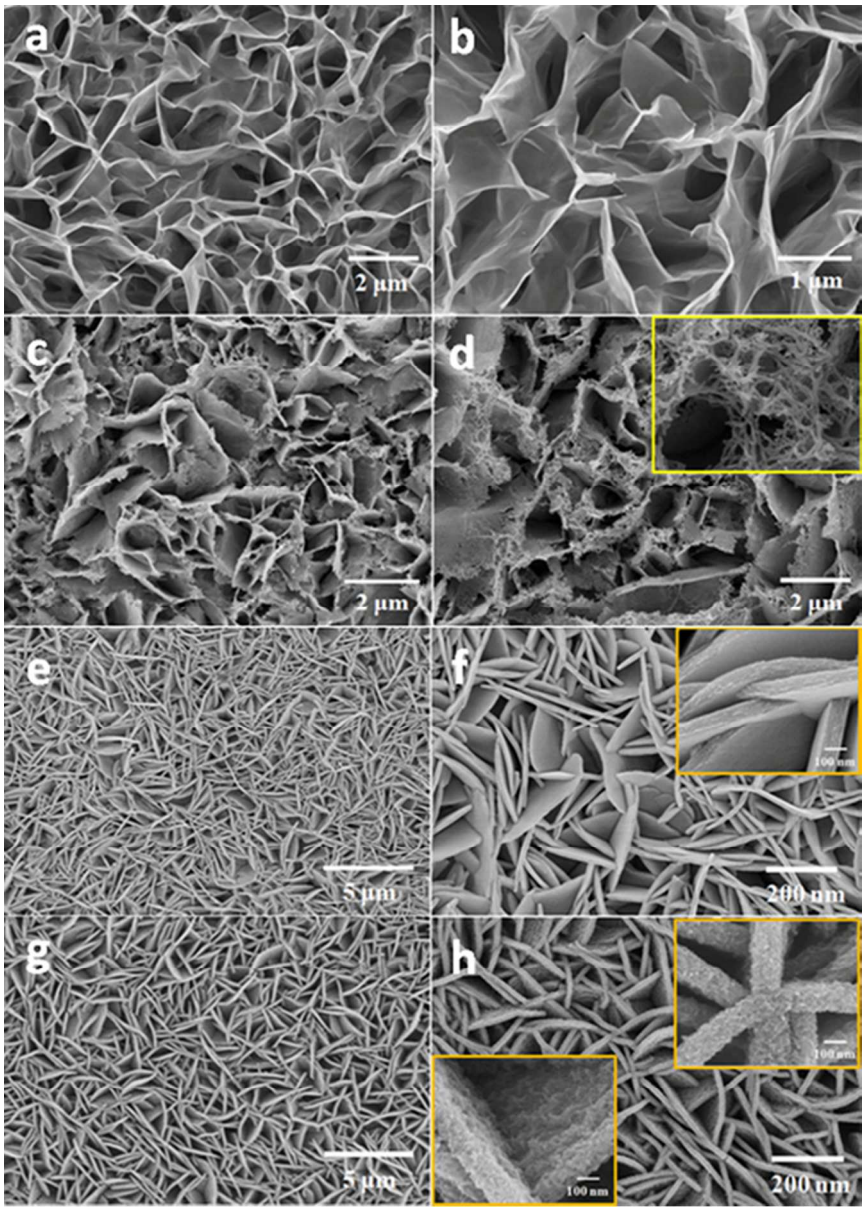

Fig. 5 (a, b) FESEM images of NiO nanoflakes and (c, d) the corresponding NiO/PANI nanohybrid composite; (e, f) FESEM images of NiO nanoplates array and (g, h) the corresponding NiO/PANI nanoarrays; the insets of (d), (f) and (h) show partial enlarged views.
53x74mm (300 x 300 DPI)

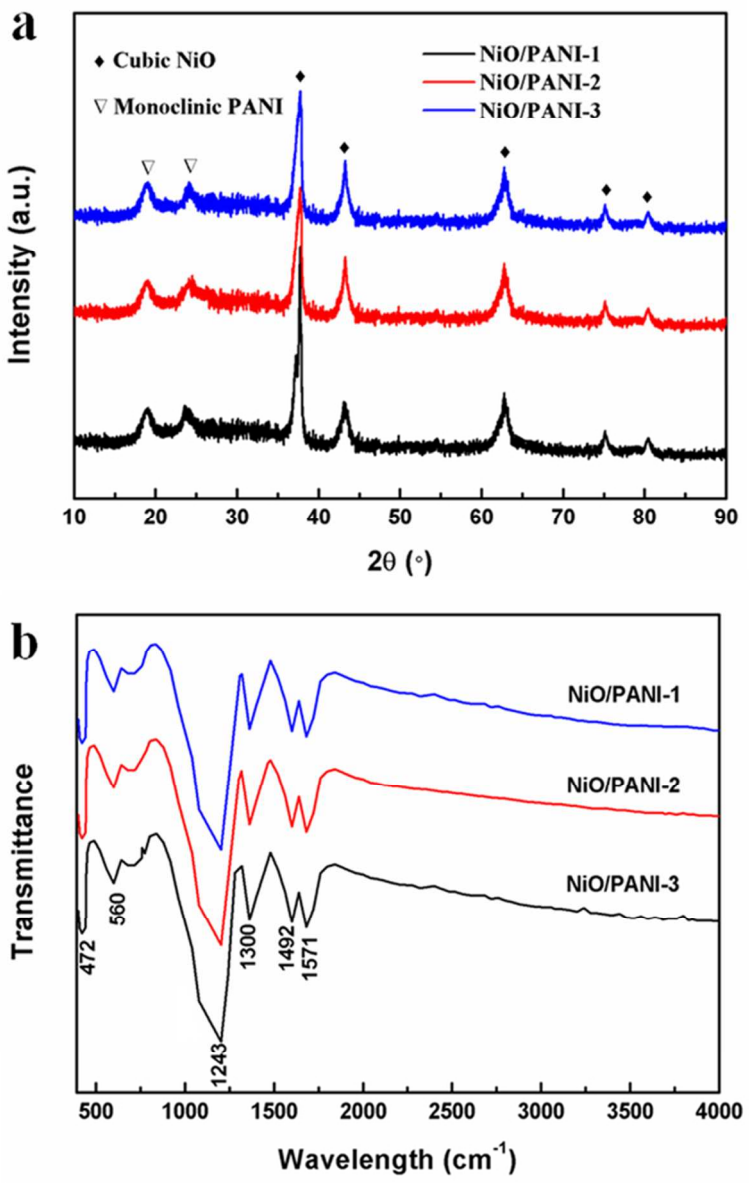

Fig. 6 (a) XRD patterns and (b) FTIR spectra for NiO/PANI-1, NiO/PANI-2 and NiO/PANI-3 nanohybrids, respectively.
54x84mm (300 x 300 DPI)

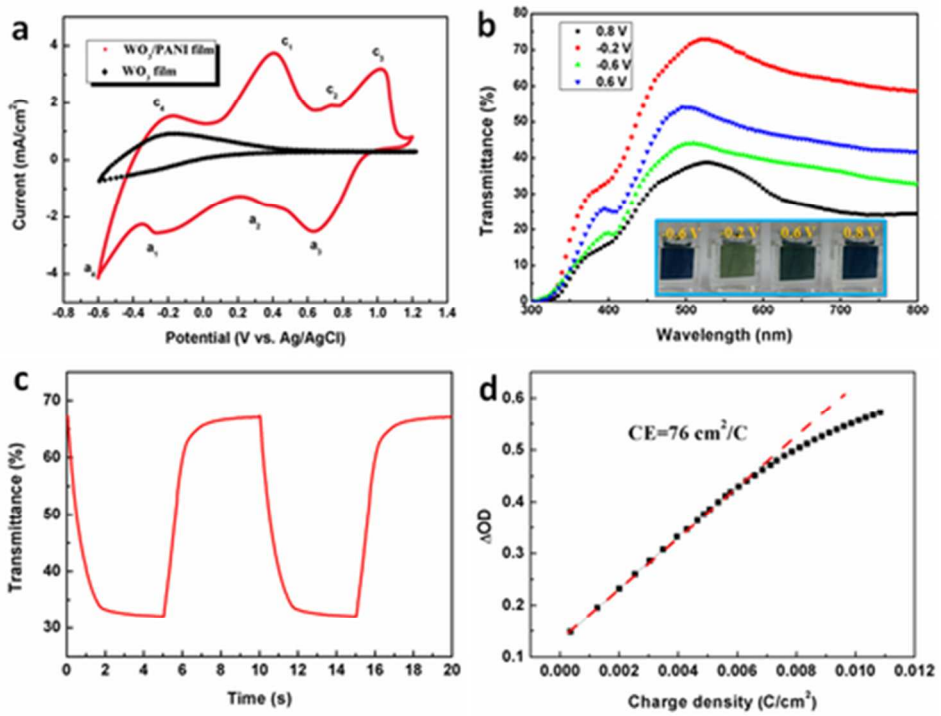

Fig. 7 (a) Cyclic voltammetry curves of pure WO_3 and WO_3/PANI nanoarrays measured in 1.0 M lithium perchlorate–PC solution with a sweep rate of 20 mV/s between -0.6 and 1.2 V; (b) transmittance spectra of WO_3/PANI nanoarrays under different voltages, with inset showing the digital photos of WO_3/PANI nanoarrays under different voltages; (c) Switching time characteristics for WO_3/PANI nanoarrays measured at 632.8 nm between -0.2 and 0.8 V; (d) ΔOD variation with respect to the charge density for WO_3/PANI nanoarrays.
40x30mm (300 x 300 DPI)

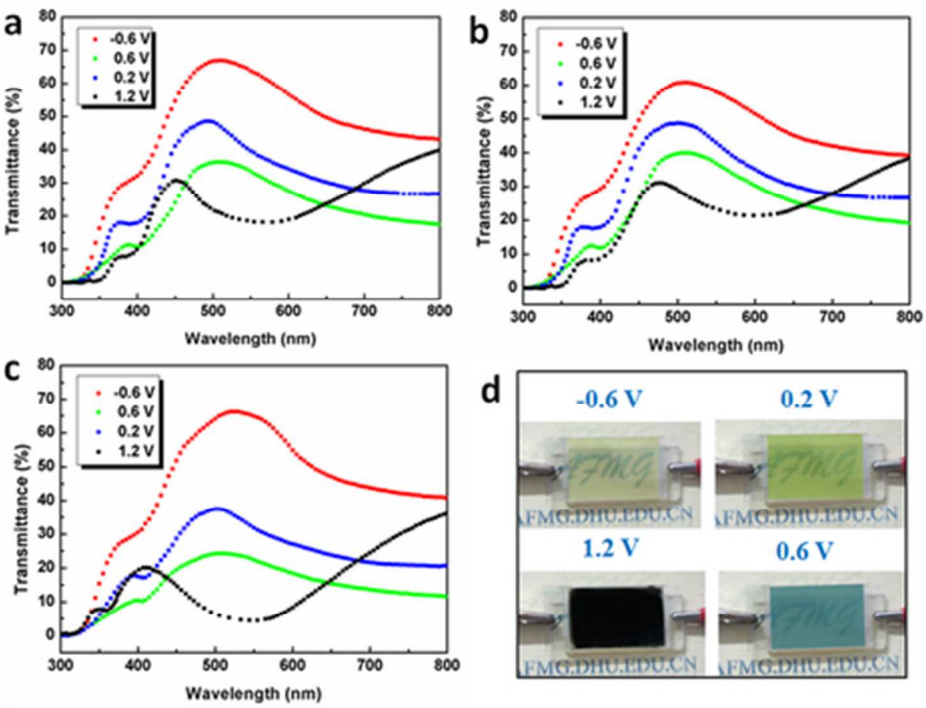

Fig. 8 (a-c) Transmittance spectra for NiO/PANI-1, NiO/PANI-2 and NiO/PANI-3 nanohybrids under different voltages, respectively; (d) digital photos of NiO/PANI-3 under different voltages.
40x31mm (300 x 300 DPI)

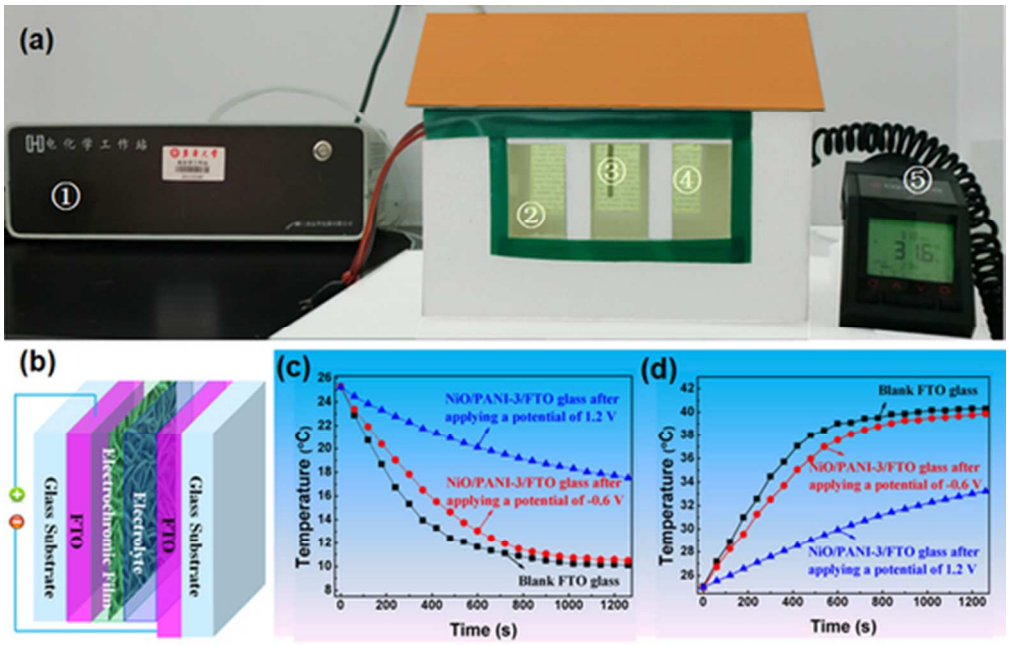

Fig. 10 (a) Photographic illustration of the testing system, 1: electrochemical workstation, 2 and 4: test windows installed in the front and back of the room, respectively, 3: temperature probe, and 5: portable thermometer; (b) scheme of the test windows; (c) and (d) temperature dependence on time for NiO/PANI-3 coated FTO glass with the temperature of thermostatic chamber fixed at 10 and 40 °C, respectively.
45x29mm (300 x 300 DPI)

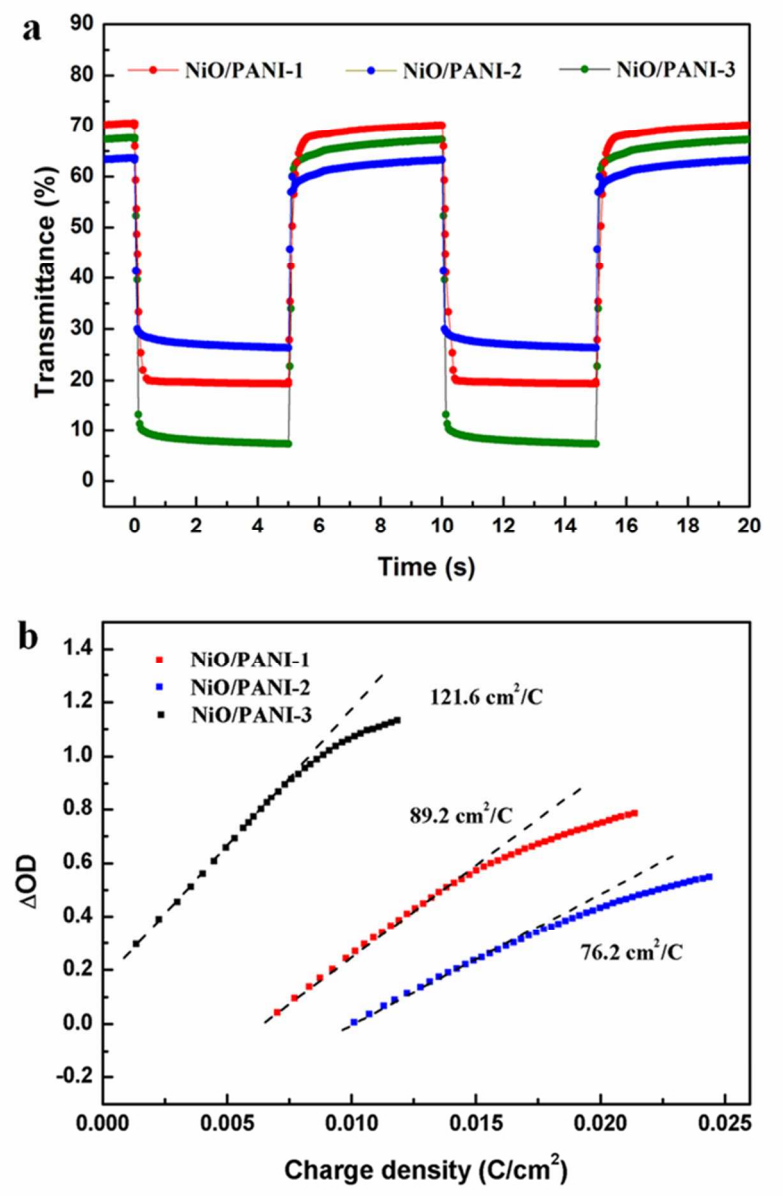

Fig. 9 (a) Switching time characteristics for NiO/PANI nanohybrids measured at 632.8 nm between -0.6 and 1.2 V; (d) ΔOD variation with respect to the charge density for NiO/PANI nanohybrids.
53x81mm (300 x 300 DPI)

Graphical Abstract

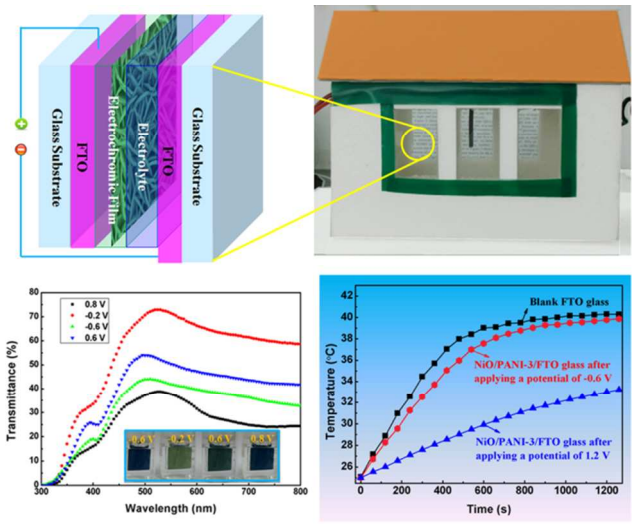

Excellent electrochromic performances of high-quality metal oxide/conducting polymer hierarchical nanoarrays are prepared using a powerful solution-based method. The application of the hybrid nanoarrays coated FTO glass causes a temperature difference of about 7 °C under different ambient temperatures, making it very attractive for potential applications in energy-saving smart windows.

Supporting Information for

Controllable Growth of High-Quality Metal Oxide/Conducting Polymer Hierarchical Nanoarrays with Outstanding Electrochromic Properties and Solar-Heat Shielding Ability

Dongyun Ma,[a,d] Guoying Shi,[c] Hongzhi Wang,[a] Qinghong Zhang,[b] and Yaogang Li*[b]*

[a] *State Key Laboratory for Modification of Chemical Fibers and Polymer Materials, College of Materials Science and Engineering, Donghua University, Shanghai 201620, P. R. China. Fax: +86-021-67792855; Tel: +86-021-67792881; E-mail: wanghz@dhu.edu.cn*

[b]*Engineering Research Center of Advanced Glasses Manufacturing Technology, Ministry of Education, College of Materials Science and Engineering, Donghua University, Shanghai 201620, P. R. China. Fax: +86-021-67792855; Tel: +86-021-67792526; E-mail: yaogang_li@dhu.edu.cn*

[c]*College of Chemistry, Chemical Engineering and Biotechnology, Donghua University, Shanghai 201620, China.*

[d]*School of Materials Science and Engineering, Shanghai University, Shanghai 200444, People's Republic of China.*

For the preparation of the organic part of hybrid materials, electrochemical polymerization is indeed an attractive method because the morphologies of polymers can be controlled through simple adjustment of the parameters of the synthetic procedure. Fig. S1 shows the FESEM images of PANI films prepared using different electropolymerization procedures. It can be seen that PANI films with amorphous morphologies were obtained under both potentio- and galvanostatic procedures, while the crystalline PANI nanorod-like films were grown using a potential cycling protocol. For the amorphous PANI, polymeric macromolecules are too big to penetrate into the pores of a nanostructured metal oxide matrix (especially if it is already partially loaded), resulting in insufficient pore filling. The net result is that the organic component resides dominantly at the upper areas of the nanoporous metal oxides.

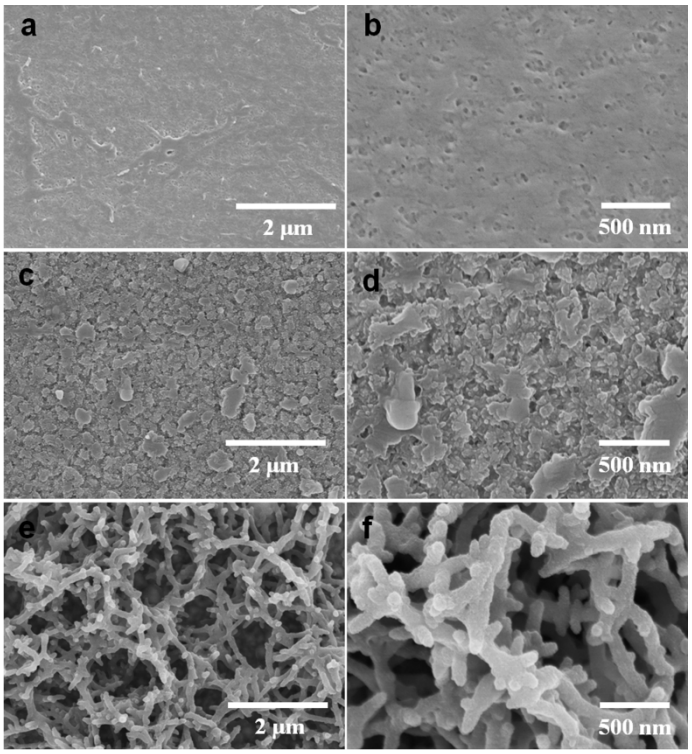

Fig. S1 FESEM images of PANI films prepared using (a, b) potentiostatic procedure at 1.2 V for 2 min, (c, d) galvanostatic procedure with current density of 0.5 mA/cm^2 for 10 min and (e, f) potentiodynamic cycle at a sweep rate of 100 mV/s for 100 cycles between -0.6 and 1.2 V.

Fig. S2 shows the XRD patterns of the porous NiO films prepared in the reaction

solution containing different structure-directing agent and solvent. From the XRD patterns, it was confirmed that all the diffraction peaks of the samples were indexed to the cubic NiO phase (JCPDS no. 04-0835).

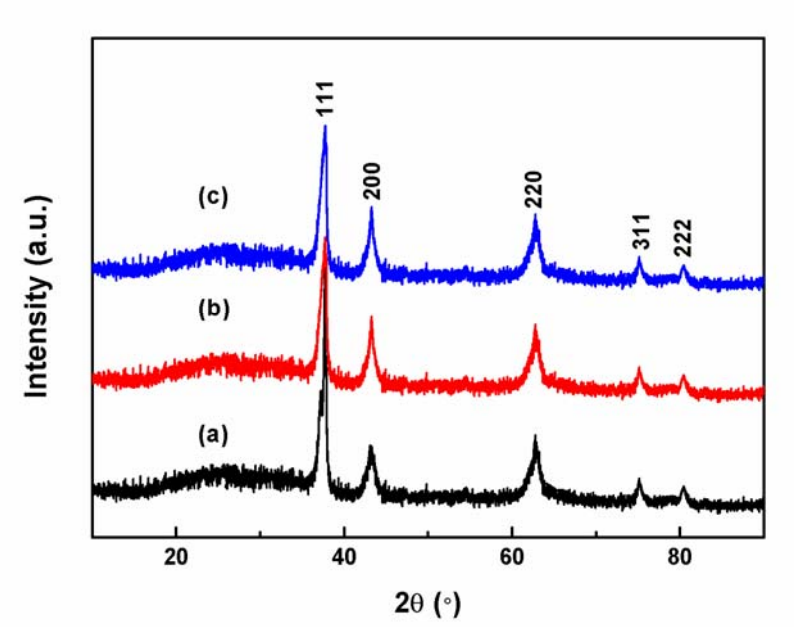

Fig. S2 XRD patterns of porous NiO films synthesized with (a) addition of 0.6 g urea, where water was used as solvent, (b) addition of 0.6 g urea, where ethanol was used as solvent and (c) addition of 0.3 g $K_2S_2O_8$ and 3 mL NH_3H_2O, where water was used as solvent,.

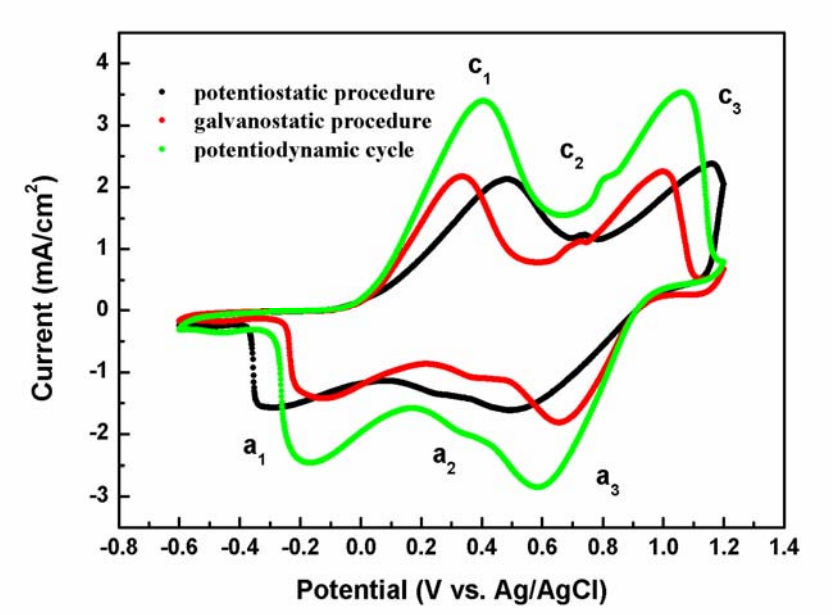

Fig. S3 Cyclic voltammetry curves of PANI films deposited by potentiostatic, galvanostatic procedures and potentiodynamic cycle.

Fig. S3 shows the cyclic voltammetry curves of PANI films deposited by potentiostatic, galvanostatic procedures and potentiodynamic cycle, respectively, which have three typical redox peaks (c_1/a_1, c_2/a_2 and c_3/a_3). The redox couples c_1/a_1 and c_3/a_3 correspond to the change between leucoemeraldine salt (LS) and emeraldine salt (ES), emeraldine salt (ES) and pernigraniline salt (PS) of PANI with anion doping/dedoping processes, respectively. The redox couple c_2/a_2 can be ascribed to hydrolysis products of PANI due to over-oxidation at comparatively high potential.

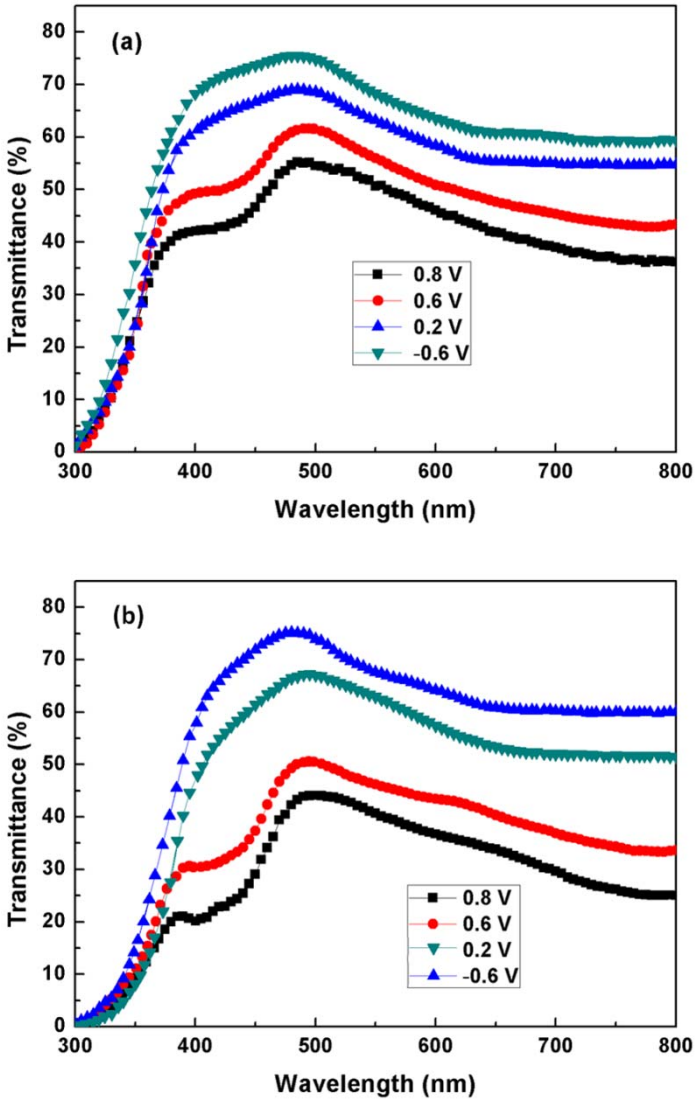

Fig. S4 Transmittance spectra of PANI films under different voltages: (a) PANI films prepared by potentiostatic procedure, (b) PANI films prepared by galvanostatic procedure.

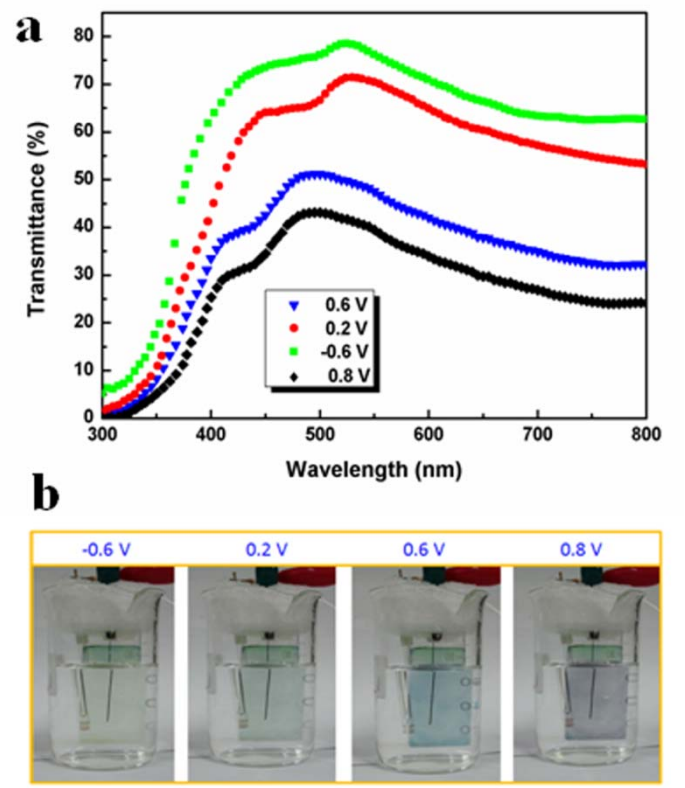

Fig. S5 (a) Transmittance spectra of PANI films prepared by potentiodynamic cycle under different voltages, (b) the corresponding digital photos of PANI films under different voltages.

The as-prepared single PANI films show rich reversible color changes ranging from yellow, green, and blue to purple under different applied potentials (Fig. S5b). However, the hybrid WO_3/PANI or NiO/PANI films show more obvious color changes under different voltages (Fig. 5b and Fig. 6d in the article) than the single PANI films because the porous oxides provide not only a stable mechanical support for the active PANI but also a template for homogeneous coverage of PANI, leading to a synergistic electrochromism effect. The corresponding optical changes of the PANI films are recorded by the transmittance spectra (as shown in Fig. S4 and Fig. S5b). According to the definitions for the optical modulation in the article, the maximum values of 22%, 26% and 32% are reached between -0.6 and 0.8 V for PANI films deposited by potentiostatic, galvanostatic procedures and potentiodynamic cycle, respectively.

The switching times and coloration efficiency for the PANI films prepared by potentiodynamic cycle were measured and shown in Fig. S6. The response times

under the voltages of -0.6 and 0.8 V are found to be 300 and 500 ms, respectively, faster than those of the WO_3/PANI films (500 and 800 ms, respectively). The poor conductivity of inorganic container (WO_3 is insulating, especially at positive potential) is responsible for the slow switching speed of the WO_3/PANI films. The calculated CE value of the PANI films is 49.2 cm^2 C^{-1}, which is much lower than those of both the WO_3/PANI and NiO/PANI films.

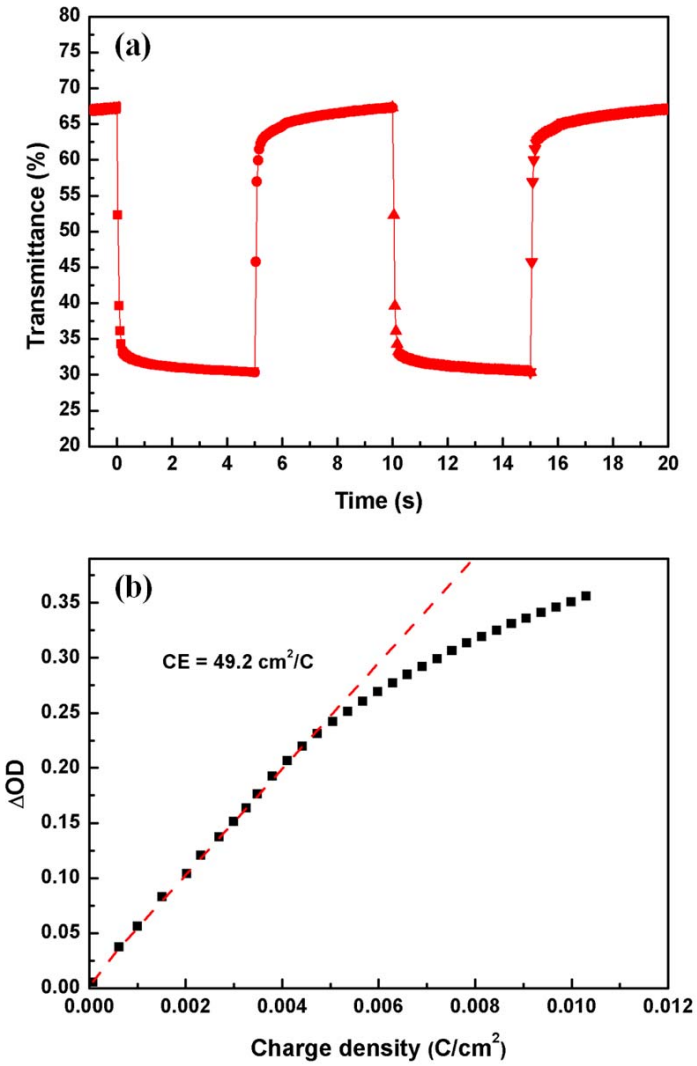

Fig. S6 (a) Switching time characteristics measured at 632.8 nm between -0.6 and 0.8 V and (b) ΔOD variation with respect to the charge density for the PANI films prepared by potentiodynamic cycle.

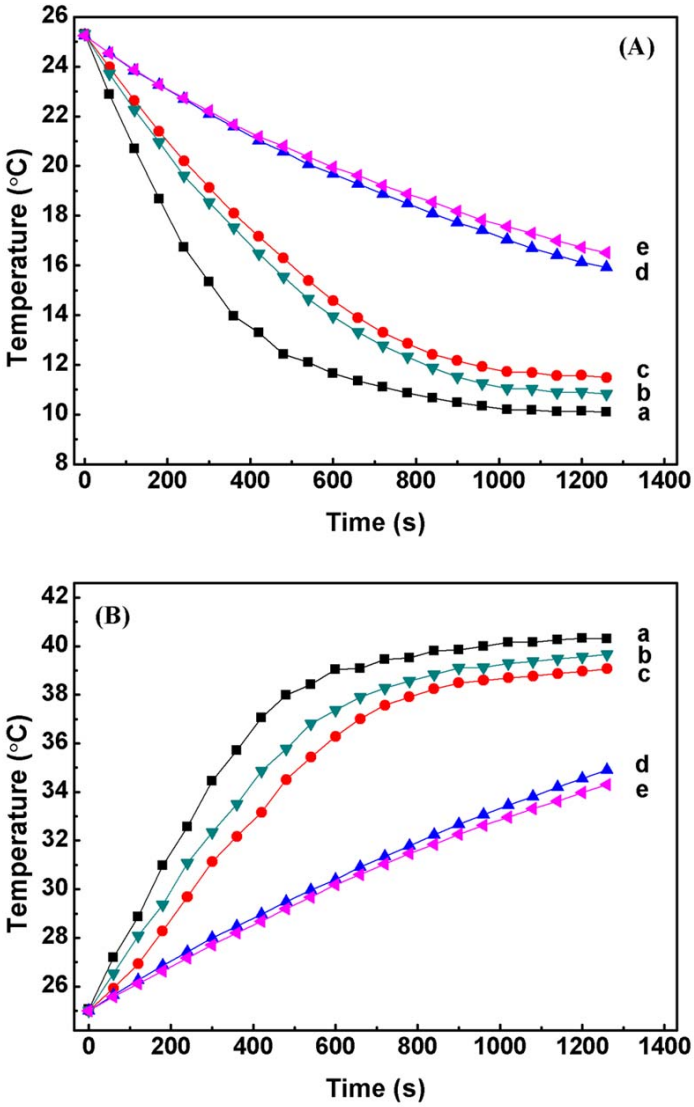

Fig. S7 (A) Temperature dependence on time for NiO/PANI coated FTO glass with the temperature of thermostatic chamber fixed at 10 °C, a: blank FTO glass, b and d: NiO/PANI-2/FTO glass after applying potentials of -0.6 V and 1.2 V, respectively, c and e: NiO/PANI-1/FTO glass after applying potentials of -0.6 V and 1.2 V, respectively; (B) Temperature dependence on time for NiO/PANI coated FTO glass with the temperature of thermostatic chamber fixed at 40 °C, a: blank FTO glass, b and d: NiO/PANI-2/FTO glass after applying potentials of -0.6 V and 1.2 V, respectively, c and e: NiO/PANI-1/FTO glass after applying potentials of -0.6 V and 1.2 V, respectively.

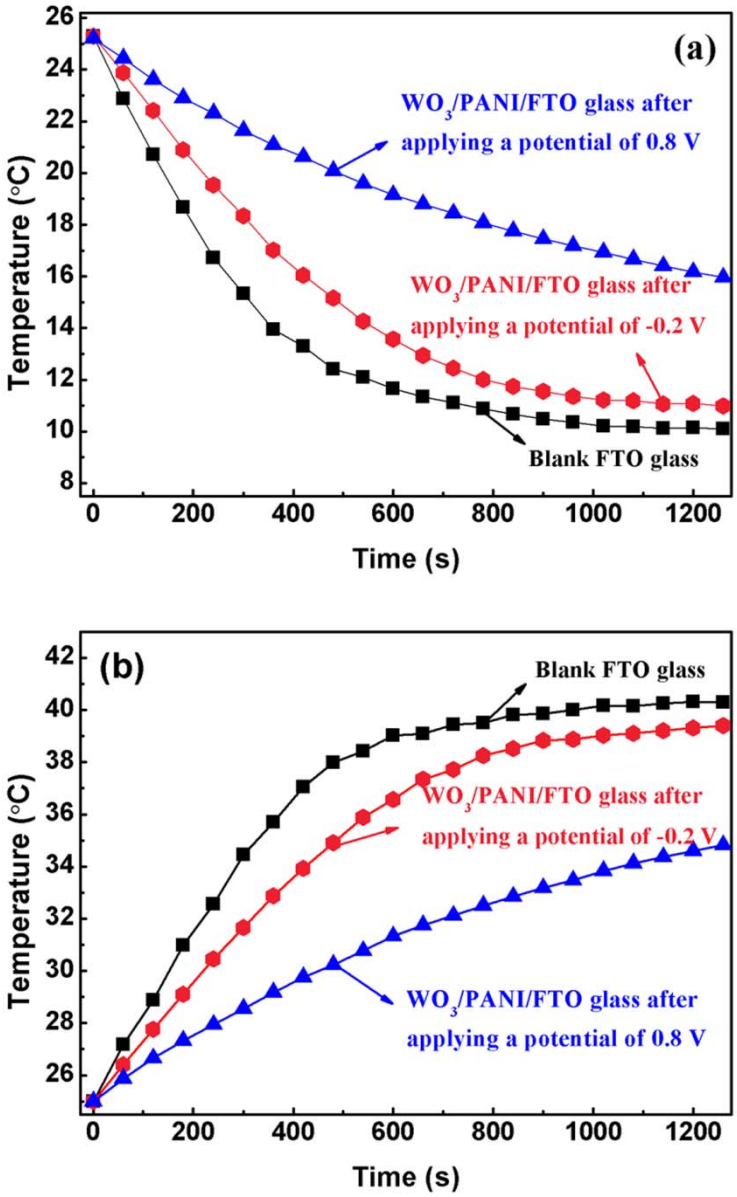

Fig. S8 (a) and (b) temperature dependence on time for WO_3/PANI coated FTO glass with the temperature of thermostatic chamber fixed at 10 and 40 °C, respectively.

In this work, we have constructed a model house (as mentioned in the article) to evaluate the solar-heat shielding ability of WO_3/PANI and NiO/PANI hybrids coated FTO glass. Fig. S7 and S8 show temperature dependence on time for NiO/PANI-1, NiO/PANI-2 and WO_3/PANI coated FTO glass with the temperature of thermostatic chamber fixed at 10 and 40 °C, respectively. The values calculated from Fig. S7 indicate that the application of the NiO/PANI-1 and NiO/PANI-2 coated FTO glass causes temperature differences of about 4.7 and 4.2 °C (when the outer room (thermostatic chamber) temperature fix at 10 °C) compared with the blank FTO glass,

respectively. In another case (when the outer room temperature fix at 40 °C), temperature reduction of about 4.6 and 4.3 °C are achieved for the NiO/PANI-1 and NiO/PANI-2 coated FTO glass, respectively. The values calculated from Fig. S8 indicate that the application of the WO_3/PANI coated FTO glass causes a temperature difference of about 4.4 °C (when the outer room temperature fix at 10 °C) compared with the blank FTO glass. In another case (when the outer room temperature fix at 40 °C), a temperature reduction of about 4.2 °C is achieved for the WO_3/PANI coated FTO glass.

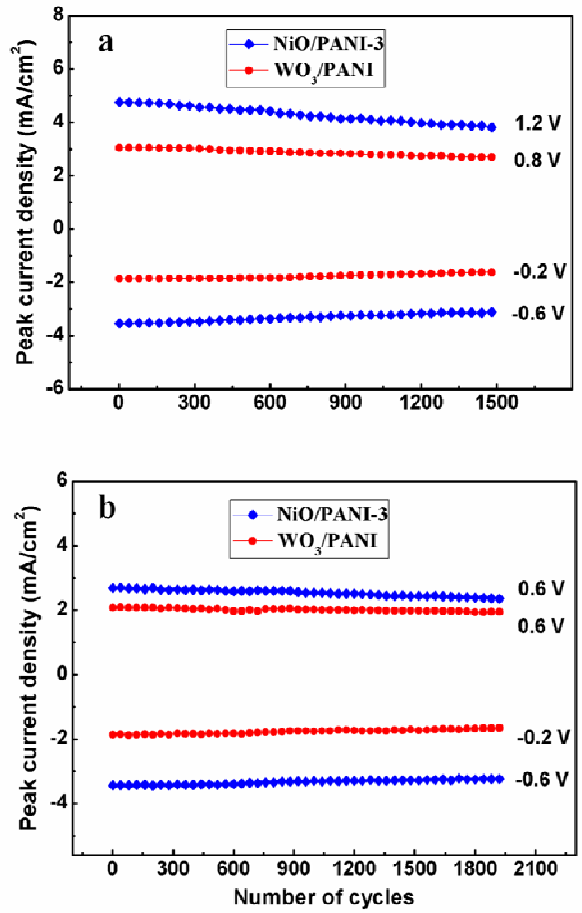

Fig. S9 Peak current evolution of the WO_3/PANI and NiO/PANI-3 films during the step chronoamperometric cycles under different potentials.

The cycle stability of the WO_3/PANI and NiO/PANI-3 films is characterized by chronoamperometry using the corresponding square potentials mentioned in the manuscript. The evolution of corresponding redox peak currents is presented in Fig. S9. For WO_3/PANI films, the degradations of the peak currents at 0.8 and -0.2 V after 1500 cycles are 13.5% and 12.7%, respectively. For NiO/PANI-3 films, the degradations of the peak currents at 1.2 and -0.6 V after 1500 cycles are 21% and

13.1%, respectively. It is confirmed that the PANI is not stable as a result of benzoquinone formation by hydrolysis during cycling, especially under a potential higher than 0.7 V. We therefore have also investigated the cycling stability of EC devices based on WO_3/PANI and NiO/PANI films at a low oxidation potential of 0.6 V (as shown in the Fig. S9b). The degradations of the peak currents at 0.6 V after 2000 cycles for the WO_3/PANI and NiO/PANI-3 films based on EC devices are 6% and 9.3%, respectively. Obviously, the cycle stability of the EC devices assembled by WO_3/PANI and NiO/PANI-3 films is highly enhanced when a low oxidation potential was applied.